TECHNISCHE UNIVERSITÄT WIEN
Vienna | Austria

ATOMINSTITUT

Master Thesis

Comparison of measurements of filters exposed to high flow environmental air using an HPGe and a LaBr detector

Technische Universität Wien - Atominstitut

Franz-Stephan Strobl, BSc

0826132

January 2016

Supervisor: Ao.Univ.Prof. Dipl.-Ing. Dr.techn. Helmuth Böck

Senior Scientist Dipl.-Ing. Dr.techn. Johannes Sterba

Inhalt

Abstract

After the accident of the nuclear power plant Fukushima Dai-Ichi, which released large amounts of radionuclides into the air, the necessity for online monitoring systems for the international monitoring stations of the CTBTO became apparent. Since these stations are high air flow sample stations a scenario of 10 Bq/m³ of I-131 in the air will accumulate an activity of 140 000 Bq on the filter during the 24 hour long exposure. To mitigate the danger from such filters for the operators and to gain a faster alert if high activity concentrations are present in the air, compared to the current 52 hours after collection start, the Provisional Technical Secretariat in Vienna started a project to equip the air sampler stations with a low resolution detector. The chosen detector material is the $LaBr_3$:Ce which is provided in the BrilLanCe380 detector produced by Saint-Gobain. Its main advantages are its high resolution of 2.5% at 662 keV which allows a separation between I-131 (at 364.5 keV) and Pb-214 (at 351.9 keV). Also the multiplet of 1473 keV, from the intrinsic La-138 content of the detector, and 1441 keV from K-40 can be used for an automated internal quality control which stabilises the spectrum against environmental temperature changes and automatically applies an energy calibration to the measured spectra. During this study the sensitivity of the new LaBr system regarding the capability to detect the naturally occurring radionuclide Be-7, the minimal detectable concentration of the nuclear event indicators I-131 and Ba-140 and the ability to separate the 351.9 keV and 364.5 keV peaks of I-131 and Pb-214 will be assessed. The LaBr spectra were acquired alongside the normal collection process of the air sampler and compared to the results of an HPGe detector that were acquired after the end of the 24 hour exposure of the filter. The acquisition time interval for the LaBr spectra was set to 10 minutes (144 spectra per day), but since no Be-7 peak could be measured, the acquisition time was increased to one hour per spectra (24 spectra per day). The increase in acquisition time did not enable the detection of Be-7. The lowest calculated minimal delectable concentration (MDC), recorded in the last hour after a 62 hour filter exposure, showed a value of 1.68E-02 Bq/m³. The HPGe detector recorded an activity concentration of 5.85E-03 Bq/m³ for this filter. Therefore the detection of the natural radionuclide Be-7 in its usual concentrations is not possible with the LaBr detector system. The minimal detectable concentration of I-131 and Ba-140, even for the highest recorded minimal detectable concentration values right at the start of the measurement of 1.39E-01 Bq/m³ and 6.47E-01 Bq/m³, are low enough to detect a situation as in the assumed scenario in the first hour. This

ensures the protection of the station operators and enables an early warning for the CTBTO. The analysis of the peak position of Pb-214 showed a maximum deviation of 1.24 keV from the correct value and no correlation with the temperature of the LaBr detector, which shows that the spectrum stabilisation via the La-138/K-40 multiplet works appropriately. The measured full width half maximum (FWHM) variations of the Pb-214 peak on the other hand, which cannot be compensated by the stabilisation system, show a correlation to detector temperature and therefore the temperature of the environment. The results of the FWHM reached values above 15 keV a few times and the detector temperature reaches as high as 36.6 °C. Nevertheless FWHM reaches values as low as 12.2 keV and the average FWHM values of 13.5 keV is still enough, if only barely, to allow a separation of I-131 and Pb-214.

Zusammenfassung

Nach dem Unfall im Atomkraftwerk Fukushima Dai-Ichi, der die Freisetzung einer großen Menge von Radionukliden in die Luft zur Folge hatte, wurde die Notwendigkeit eines online Überwachungssystems für die internationalen Messstationen der CTBTO deutlich. Da diese Stationen einen hohen Luftstrom zum Sammeln der Proben haben, erreichen sie nach der gesamten Probensammelzeit von 24 Stunden für ein Szenario von 10 Bq/m³ von I-131 in der Luft einen Aktivitätswert von 140 000 Bq auf dem Filter. Um die Gefahren, die von solchen Filtern ausgehen, zu minimieren und einen frühzeitigeren Alarm für hohe Aktivitäten in der Luft, verglichen mit den derzeitigen 52 Stunden nach Beginn des Sammelprozesses, zu erhalten hat das Provisorische Technische Sekretariat in Wien ein Projekt begonnen, welches die Sammelstationen selbst mit einem niedrig auflösendem Detektor ausstatten soll. Die Wahl für das Detektormaterial fiel auf $LaBr_3$:Ce welches in Form des BrilLanCe 380 Detektors von Saint-Gobain hergestellt wird. Einer der Hauptvorteile dieses Detektors ist seine hohe Auflösung von 2.5% bei einer Energie von 662 keV, die es ermöglicht zwischen I-131 (bei 364.5 keV) und Pb-214 (bei 351.9 keV) zu unterscheiden. Des Weiteren kann mit Hilfe des Multiplets 1473/1441 keV, erzeugt durch K-40 und das intrinsische im Detektormaterial enthaltene La-138, eine automatische interne Qualitätskontrolle zur Stabilisierung des Spektrums gegen Schwankungen in der Umgebungstemperatur durchgeführt werden. Diese erzeugt auch automatisch die Energie-Kalibrierung für die aufgezeichneten Spektren. Durch diese Studie soll die Sensitivität des neuen LaBr-Systems bezüglich seiner Fähigkeit zur Erfassung des natürlich vorkommenden Radionuklids Be-7, der minimal detektierbaren Konzentration von I-131 und Ba-140, welches Indikatoren für Nukleare Ereignisse sind, und seiner Leistungsfähigkeit bei der Unterscheidung zwischen den Spektrallinien bei 351.9 keV und 364.5 keV von I-131 und Pb-214 festgesellt werden. Die Spektren des LaBr-Detektors werden während des normalen Sammelfortgangs aufgezeichnet und die Ergebnisse werden mit denen eines HPGe-Detektors verglichen, welcher den Filter nach der abgeschlossenen Sammelzeit von 24 Stunden vermisst. Die Messzeit der LaBr Spektren lag bei 10 Minuten (144 Spektren pro Tag), da bei dieser Einstellung aber keine Be-7 Spektrallinie messbar war wurde die Messzeit auf eine Stunde erhört (24 Spektren pro Tag). Die Erhöhung der Messzeit ermöglichte es nicht Be-7 in den Spektren des LaBr-Detektorsystems zu erkennen. Die minimal detektierbare Konzentration von I-131 und Ba-140 ist aber immer, selbst für die höchsten gemessenen Werte vom 1.39E-01 Bq/m³ und 6.47E-01 Bq/m³ niedrig genug, um

auftretende Aktivitätskonzentrationen wie im obigen Szenario angenommen von der ersten Stunde an zu erkennen. Dies ermöglicht den Schutz des Messstationen Personals und lässt eine frühzeitige Warnung der CTBTO zu. Die Analyse der Spektrallinienposition zeigte eine maximale Abweichung von 1.24 keV vom korrekten Wert und zeigt keine Korrelation zur Temperatur des LaBr-Detektors. Dies bestätigt, dass die Stabilisierung des Spektrums mittels des La-138/K-40 Mutiplets korrekt arbeitet. Die gemessene Schwankung der Halbwertsbreite (FWHM) von Pb-214 zeigt einen Zusammenhang mit der Detektor- und damit der Umgebungstemperatur. Die Ergebnisse der FWHM überschreiten einige Male Werte von 15 keV, wobei die gemessenen Detektortemperaturen 36.6 °C erreichen. Es werden aber auch niedrige Werte von bis zu 12.2 keV gemessen und der Mittelwert der FWHM von 13.5 keV ermöglicht gerade noch eine Unterscheidung zwischen I-131 und Pb-214.

1 Introduction and Motivation

This study compares the results of the measurements of an air filter exposed for 24 hours and measured every hour during this time period by a LaBr detector, with a measurement obtained with an HPGe detector after the exposure. It will be assessed if activity of naturally occurring isotopes are matching in both measurement setups. The measurement time of the LaBr detector was increased to one hour after results from measurements with the originally planned timeframe of 10 minutes showed that the sensitivity was too low to detect the naturally occurring radioisotope Be-7. Further, the minimal detectable concentration (MDC) of the radioisotopes Be-7, I-131, and Ba-140 will be compared.

The necessity for an online measurement with frequent analysis is to ensure the station operators' health and safety and was recognized after the accident in Fukushima caused extremely high activities on the exposed filters. Because of the high air flow rate of the International Monitoring Stations (IMS) of the Comprehensive Test Ban Treaty Organization (CTBTO) the accumulated activity on the filter could potentially cause radiological dangers for the station operators although the radioactivity in the air is still below hazardous levels. The assumed scenario for a severe case is an activity concentration of I-131 of 10 Bq/m^3 in the air. The average air flow volume of an IMS station is between 700 and 1000 m^3 per hour. During the standard collection time of 24 hours the activity on the exposed filter would accumulate to 140 000 Becquerel. Apart from the dangers of the filter the first results from the filter analysis are not available until more than 50 hours after the collection started. Therefore members of the Provisional Technical Secretariat of the CTBTO in Vienna started to examine the possibility of an online early warning system that monitors the filter during the collection time with a low resolution LaBr detector. The specific LaBr detector was chosen because its resolution allows to distinguish between the radioactive Iodine isotope 131 and the Radon daughter product Lead 214. Also the LaBr detector has a sensitivity that is several orders of magnitude higher than conventional dose monitoring devices such as a Geiger-Müller dose rate meter. The new LaBr system shall warn the station operator about radiological hazards deriving from the filter and give the CTBTO an early notification to react to such situations.

2 Basics of gamma spectrometry[1]

The process of gamma emission is similar to the de-excitation of an electron in the electron shell. The process itself is, unlike the alpha or beta decay, not a change in number or type of nucleons, although it often appears after these decay processes, but a way to lose the surplus of energy for the nucleus. Excited nucleus states often appear after decay of an unstable nuclide. Unstable nuclides have a mismatched number of neutrons and protons in the nucleus. Not all the energy released by the mass defect is converted into kinetic energy of the decay products, the residual energy appears as excitation of the decay product's nucleus. Such a nuclear decay process can happen in three ways, which will be described in the following subchapters.

2.1 Nuclear decay processes

2.1.1 Beta decay

The energy of the nucleus is reduced through an isobar transition; leaving the atomic mass number (A) constant. Depending on what nucleon causes the unstable surplus, neutrons change into protons leading to β^- decay or protons changing into neutrons leading to β^+ decay.

β^- (negatron) decay

This decay happens if the nuclide is on the neutron rich side of stability.

$$ {}^{A}_{Z}X \xrightarrow{n \to p} {}^{A}_{Z+1}Y + \beta^- + \overline{\nu} $$

A… atomic mass number A = N + Z; N… number of neutrons in the nucleus;

Z… atomic number, number of protons in the nucleus;

The beta particle β^- is an electron and $\bar{\nu}$ is an anti-neutrino. In the decay process, a neutron is converted to a proton: $n \to p^+ + \beta^- + \overline{\nu}$; changing the composition of the nucleus into a more stable condition. Nearly all the decay energy is shared between the beta particle and the anti-neutrino, therefore the energy of the beta particle can vary between zero and 100% ($E_{\beta\, max}$).

If the beta transition is made directly to the ground state of the daughter nucleus, no gamma radiation will be emitted. But beta transition to an excited state of the daughter nuclide will

[1] This chapter is based on the second edition of the book Practical Gamma-ray Spectrometry by Gilmore (2008). If other sources are used they are referred to at the concerning passage.

lead to de-excitation by gamma emission. Hence the energy of the gamma radiation is actually a property of the energy levels in the nucleus of the daughter nucleus. The de-excitation can happen via serval energy levels in the daughter nucleus; leading to several significant gamma rays emitted simultaneously (= in cascade).

β⁺ (positron) decay

This decay happens if the nuclide is on the neutron deficient side of stability.

$$ {}^{A}_{Z}X \xrightarrow{p \rightarrow n} {}^{A}_{Z-1}Y + \beta^{+} + \nu $$

The process creates a positron β^{+} (anti-electron) and a neutrino ν. The needed electron has to be created in a pair production; reducing the decay energy by 1022keV. Therefore β^{+}decay can only occur for decay energies higher than this threshold. The position created in the pair production is the β^{+} particle emitted in the formula above. Again the energy is mostly shared between the positron and the neutrino and can range from zero to 100%. The positron will be slowed down fast inside of matter and annihilate with a close electron; releasing two photons with 511.00 keV. These photons can cause an annihilation peak in the spectrum.

2.1.2 Electron capture (EC)

This is an alternative process to the β^{+}decay. The electron needed for the conversion of a proton into a neutron can also be taken from the electron shell of the nucleus by electron capture. This decay option can also occur if the decay energy is too low for a pair production process; lower than 1022 keV. The electron will usually be taken from the closest shell to the nucleus, the K shell. The vacancy in the shell is filled by a weaker bound electron, which can lead to electron cascades to gain the lowest energy constellation of the electron shell. Each of these electron rearrangements releases a small amount of energy which often appears as one or more X-rays. The released energy can also free an electron completely from the atom and thereby emit a so called Auger electron from the atom.

2.1.3 Alpha decay

Atoms with a high atomic number, over 83, usually decay through the emission of an alpha particle which is a Helium nucleus ${}^{4}_{2}He^{2+}$.

$$ {}^{A}_{Z}X \xrightarrow{\alpha\ emission} {}^{A-4}_{Z-2}Y + {}^{4}_{2}He + Q $$

This reduces the atomic mass (A) by four units and the atomic number by two units. The energy (Q) from the mass defect is distributed between the reaction products and as no additional neutrino particle is produced, the alpha particle has a specific, characteristic energy. However only a small fraction, if any at all, of the daughter nuclides are in a higher state than the ground state. (No de-excitation through emission of gamma radiation.)

2.1.4 Spontaneous fission

This is a natural decay process for heavy nuclides, where they split into two fragments and a variable number of neutrons. The fission products of a spontaneous fission are usually on the neutron rich side of the stability line and therefore undergo β^- decay, leading to the emission of gamma radiation.

2.2 Gamma radiation origins

The energy of gamma radiation lies between 10 keV (~10^{-10} m) and 10 000 keV (~10^{-13} m) in the energy spectrum of electromagnetic waves. Therefore there is an overlap with the higher-energy X-rays, which range up to 100 keV.

The possible energy levels of a nucleon are similarly restricted as for the electrons in the electron shell model. The nuclear shell model considers the nucleons as quantum objects. Although they are assumed to be independent from one another, they move in an average potential that is generated by the rest of the nucleons in the nucleus. The allowed energy levels follow the Pauli Exclusion Principle and can be calculated by solving the Schrödinger equation for such a single independent nucleon in an oscillator potential (Faber, 2011).

The possible movements and its probability between the nucleus shells derive from the origin of the energy states of the nucleus, which come from the charge and current distribution in the nucleus. The charge distribution creates an electric moment, which affects the protons; the current distribution creates a magnetic moment affecting protons and neutrons. The electric and magnetic moment can be expressed in a multipole expansion, the dipole moment corresponds to the first shell (E1 and M1) the quadrupole moment to the second most inner shell (E2 and M2) and so on. Additionally there is also the parity of the wave function and its possibly changes that defines the possible transitions. The energy of the nuclear levels is not infinitely precise, it is inversely related to its lifetime via the Heisenberg Uncertainty principle. However this uncertainty in the emitted gamma energy is

not significant compared with the precision of the measurement (>10^{-3} eV for the 1332.5keV peak of Co-60). The lifetime of an excited state is less than 10^{-12} seconds, the photon emission happens therefore nearly instantly after the nucleus enters the excited state.
If two radionuclides decay to the same daughter nuclide the main energy line for them is identical. Therefore the identification of the original radionuclide is obstructed.

The main competing process to gamma emission is internal conversion. The excitation energy of the nucleus is transferred to an electron that gets ejected thereby. This is followed by electron capture to fill the vacancy and a variety of X-rays and Auger electrons can be produced.

Apart from nucleus de-excitation there are a number of other photon sources that produce light in the gamma-spectrum:

- Annihilation radiation: Positrons annihilate and emit two photon of 511.00 keV. The positron can originate from β^- decay or from positron emitters such as Na-22. This has to be considered for example during the efficiency calibration.
- Bremsstrahlung: This X-ray radiation appears when an electron is slowed down in the Coulomb field of the nucleus. The lost energy of the electron is converted into X-radiation. This raises the background continuum of the gamma spectrum, but the background level decreases with increasing energy. (Material with a low Z number has a lower Bremsstrahlung production.)
- Prompt gammas: These are gamma-rays produced in a nuclear reaction. The produced nucleus is excited and emits a gamma-ray at a time scale of femtoseconds.
- X-rays: These are produced because of rearrangements in the electron shells of the atom that follow electron capture or internal conversion. Since the X-rays are mono-energetic the peaks generated by X-rays can help to identify elements.

2.3 Gamma ray interaction with matter

Gamma rays can interact in different ways with matter in general and the detector material and its surrounding in specific. It also has to be considered that, as already mentioned, there is an overlap between gamma radiation and X-radiation and that they are identical apart from their origin. The detection of gamma radiation, as it is an uncharged photon, needs an interaction which transfers the energy of the photon into an electric signal.

The three main processes of interaction are photoelectric absorption (dominant at low energies), Compton scattering (dominant in the mid energy region) and pair production (dominant for high energies).

2.3.1 Photoelectric absorption

The full energy of the photon is transferred to an electron. The bound electrons of the atom is ejected from its shell through this interaction with the gamma photon. The kinetic energy of the electron equals the difference of the photon energy and the binding energy of the electron. The vacancy in the shell leads to a release of further electrons through an Auger cascade process, releasing the rest of the photon energy. Or the vacancy is filled by a higher-energy electron emitting X-ray fluorescence, which can get reabsorbed and lead to further processes. It is also possible that this X-radiation escapes from the detector, especially if the event is near the surface, leading to a smaller net energy being absorbed and thereby creating an escape peak at the low-energies right next to the full energy peak.
The energy of X-ray is determined by the shell the electron is ejected from (K, L, M). The energy shells are quantified which leads to the discontinuities (absorption edges). The probability for photoelectric absorption (= attenuation) depends proportionally on the atomic number and is indirectly proportional to the energy of the gamma-ray. Therefore heavier atoms absorb gamma radiation more effectively and are better suited for detector materials.

2.3.2 Compton scattering

During the interaction of the gamma-ray with an electron a part of its energy is transferred to the electron. The amount of transferred energy depends on the scatter angle. A scatter angle of zero transfers no energy. An angle of 180° (backscattering of the gamma-ray) transfers maximum energy, which is still lower than the entire energy the gamma-ray has. The probability of Compton scattering mainly depends on the material's density, but is nearly independent of the atomic number.
Since the gamma-ray can leave the detector after some Compton scattering events and thereby only transfers some energy, a spectrum will show a Compton continuum between zero and the Compton edge.

2.3.3 Pair production

The gamma-ray interacts with the Coulomb field of the nucleus and is converted into an electron-positron pair. For this to happen the gamma-ray energy must be higher than the combined mass of the electron-positron pair of 1022 keV (511 keV for each). The remaining energy of the gamma-ray is shared equally by the electron and positron as kinetic energy, which is then transferred to the detector material as they are slowed down. Upon reaching thermal energy the positron meets an electron and annihilates, creating two 511 keV annihilation photons. This happens within one nanosecond of the pair production and therefore is recorded at the same time as the pair production by the detector, which detects the kinetic energy of the pair (gamma ray energy minus 1022 keV). The probability of pair production increases continually with the energy and is the dominant process above 10 MeV.

The total attenuation coefficient of the gamma-ray, which describes the probability that the gamma-ray will interact with the material, is the sum of these processes and has to also take incomplete interaction into consideration.

2.4 Interaction in a detector

All these processes lead to the production of primary electrons from the gamma-ray energy, which can carry nearly zero up to almost the full energy of the gamma-ray. The energy of these elections ranges from keV to MeV and, as the energy to create an electron-hole pair is in the eV region, will create many ion pairs while moving through the detector. These secondary electrons and corresponding holes are collected by the detector to produce the electric signal. But a real detector creates some more features in the spectrum due to the possibility that part of the gamma-ray energy is not absorbed in the detector. The possible interactions and their effect on the spectrum can be seen in Figure 1 and Figure 2, taken from Practical Gamma-ray Spectrometry by Gilmore (2008).

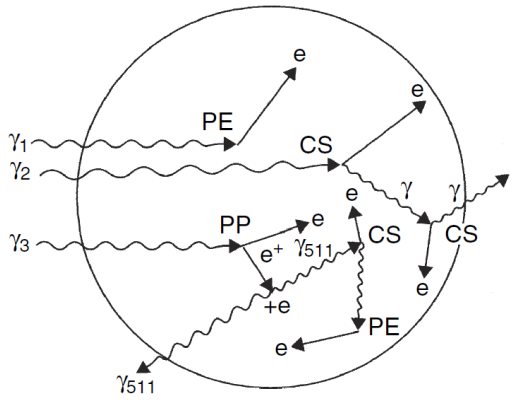

Figure 1 Possible interactions within a real detector, as shown in Figure 2.10 (Gilmore, 2008). PE Photoelectron absorption, CS Compton scattering, PP pair production, e electron, e^+ positron, γ gamma-ray.

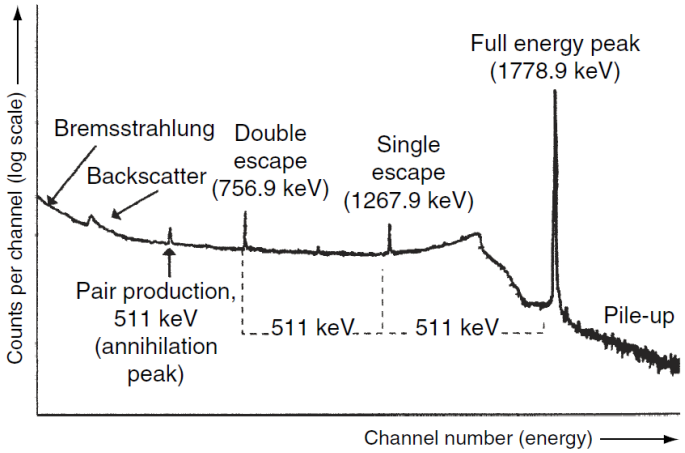

Figure 2 Example for Al-28 to illustrate the expected spectra features, as shown in Figure 2.12 (Gilmore, 2008).

The full energy peak in Figure 2 comes from the absorption of the entire gamma-ray by any number and combination of processes (γ_1 in Figure 1). The single and double escape peaks that are 511 keV and 1022 keV lower than the full energy peak come from the annihilation of a positron created in a pair production; which is followed by the escape of the scattered gamma-ray from the detector (γ_3 in Figure 1 leads to a single escape peak). Several Compton scattering processes followed by the escape of the remaining gamma energy from the detector will create the Compton continuum (γ_2 Figure 1). Additionally, true coincidence summing can occur where two gamma-rays from the sample reach the detector at the same time. This is not shown in Figure 2. The other shown event above the full energy peak comes from gamma rays that reach the detector in such a short time that they are recorded as a single event with their combined energy, called random summing or pile up.

The Bremsstrahlung comes from β^- particles (electrons) with an energy greater than 1 MeV. It superimposes the gamma-ray and increases the peak background at low energies. This effect can be decreased by placing an absorber for the beta particles between the source and the detector.

To reduce the background counts from radioactive nuclides within the environment - such as potassium 40, a primordial radionuclide, or nuclides produced by cosmic radiation - the detector is surrounded by shielding.

Other features that are visible in the spectrum derive from this very shielding that protects the detector from natural sources of gamma radiation in the surrounding. Photon interaction of the gamma-ray with the inside of the shielding can lead to photoelectric

absorption followed by the emission of characteristic X-rays. These can result in peaks in the low energy region. This is avoided by the grading of the shield with an absorber material (e.g. Cadmium for Lead shielding) or increase the space between shielding and detector. The backscatter peak is created by gamma-rays that are backscattered from the shielding and then reach the detector. This generates a broad, ill-shaped peak in the range of 200 - 300 keV. A gamma-ray hitting the shielding can also lead to pair production followed by the annihilation. One of the two 511 keV photon emitted in opposite directions can then reach the detector. This leads to an annihilation peak at 511 keV in the spectrum. (These are both visible in Figure 2.)

2.5 Electronics of a detector system

The electrical charge output of a gamma-ray detector is proportional to the gamma-ray energy. This charge has to be measured, collected, processed and stored by an electrical system before the result in form of a spectrum is available. Such a system consist of a bias supply that sweeps the electron-hole pairs from the detector. The preamplifier collects the electron-hole pairs leaving the detector and converts them into voltage pulses. The amplifier enhances the pulse shape and increases its size. The last step is a multichannel analyser (MCA) which sorts the pulses by height and counts the number of same height pulses. During the transfer of the signal from the detector to the MCA the resolution (peak width) should increase as little as possible because of electronic noise.

Bias supply: For semiconductors the detector bias supply is the critical part. The voltage simply has to lay well above the depletion voltage, in this case the stability of the supply is of no concern. The 3000-5000 volt of the bias supply that sweep the charges out of the detector reach it via the preamplifier.

Preamplifier: The preamplifier, situated before (pre) the amplifier, is often manufactured already attached to the detector, this provides the advantage that the preamplifier is cooled as well which reduces thermal electronic noise. Its purpose is to collect the charges produced in the detector and act as an interface between detector and amplifier. The charge from the detector builds up in a capacitor, the output of the preamplifier is a step wise function in voltage in which the information is carried in the height of the step.
The electronic noise from the preamplifier has a significant influence on the energy resolution of semiconductor detectors systems.

Amplifier: The amplifier converts the pulse height information, which describes the energy of the absorbed gamma-ray into individual pulses and amplifies the signal. This is done by electric filtering called shaping. To limit negative effects on the resolution by the shaping process the amplifier must also preform pole-zero cancellation and baseline restoration.
Pulse shaping: The sharp voltage increase from the preamplifier is converted via a combination of differentiators and integrators into a semi-Gaussian shaped peak. (Regarding the shaping time it has to be considered that longer times create longer amplifier output pulses. This reduces the number of pulses that can be transmitted through the system. On the other hand too short of a time will reduce the resolution.)
Pole-zero cancellation: The pulse from a normal preamplifier has a long falling tail after the sharp signal increase. Such a signal causes the integrator to produce an output to dip below the base line and then raise towards it again. The amplifier output would then have a trough that lies below the base line in its tail. This would lead to an incorrect measurement of a second pulse that follows the first one. This is corrected by a pole-zero cancellation circuit.
Baseline shift: Because there are capacitors in the shaping circuit the pulse passing through will fall under the baseline at the end. The amount of baseline shift depends on the height of the pulse. Since the MCA measures the pulse height in reference to a fixed voltage this leads to error in the measurement. This is countered by a baseline restorer in the final stage of the amplifier.
Pile-up rejection**:** Pile-up or random summing happens when more than one gamma-ray is detected almost simultaneously. If their distance is within the pulse width of the amplifier output, they cannot be recognized as two separate events. The height of the resulting pulse will be up to the combined height of the two pulses depending on their distance. This reduces the counts of those peaks and produces a new count at a random position. But the pile-up pulse is misshaped; it is wider than expected and the peak of the pulse occurs later. This misshape is used to reject such signals and the amplifier will produce no output instead of a false one. However if the two gamma-rays arrive so close to each other that the resulting pile-up peak is not misshaped but has the sum of both heights it will not be rejected and creates a summing peak.

Multichannel analyser (MCA): The output of the amplifier, which is a stream of pulses of varying heights is measured and counted by the MCA. Also pulses that are too small or big and might derive from different sources of interference are rejected. But the MCA does not

measure a continuous height distribution, it measures a consecutive sequence of height intervals. The MCA then saves the counted number of pulses according to their height, producing a spectrum. To handle all the different height intervals the pulse is converted into a digital signal after passing through the initial range-of-interest check. This is done by the analogue-to-digital-converter (ADC), which measures the pulse height and increases the corresponding counter by 1. But during this process no other pulse can be accepted. Pulses arriving during this time are not counted and therefore this is the dead time. This is compensated either by a prolonged measurement time, or by increasing count numbers according to the dead time. The resulting relation of pulse height to the corresponding channel number is not quite linear and can vary. Also it may not pass through the origin. Thus the energy calibration is necessary.
A new approach is to already convert preamplified pulse into a digital signal with a very fast ADC. All steps following the output of the spectrum are done digitally. This has several advantages such as a better temperature stability or a higher throughput of the system.

Spectrum Stabilisation: Under certain circumstances it is possible that the spectrum drifts, broadening the peaks and making it necessary to readjust the energy calibration. This is because of the effects temperature changes have on all the components of the detector and the pulse processing system. Therefore this is only an issue for detector systems which are not in a temperature-controlled environment. This is especially relevant for scintillator detectors, as their electronics are temperature sensitive and the instabilities coming from the needed high voltage. A spectrum stabilisation can be done either analogue or digitally. The analogue stabiliser uses a selected high energy single peak that is always present and monitors its shape. This is done by monitoring the counts of the channels to the left and right of the peak. If a count increase is registered at one side the gain of the amplifier is adjusted so that the peak lies between the two regions again.
The digital stabilisation is done after the recording of the spectrum. Here the spectrum drift is monitored with the spectrum results for a known low and high energy peak. The spectrum is then adjusted so that these two peaks match the corrected position.

2.6 Resolution of detectors

Since the measurement of gamma-ray energy has some uncertainties from the production of the electron-hole pairs, the collection of the charge and from the electronic noise of the pulse processing, the width of the Gaussian peak around the peak centroid, which represents the peak energy, is not a constant value.

The resolution of a detector describes the width of the Gaussian peak in the spectra it produces. It is measured by Full Width Half Maximum (FWHM) which gives the peak width of the peak at its half maximum height. Ideally the measured peaks should be as small as possible, therefore have a high resolution. High resolution enables the separation of peaks which are close in energy. If the peak centroids are more than three FWHM apart the peaks are clearly separated. If they are only 1 FWHM apart a separation is still possible with the support of spectrum analysis programs. A higher resolution also helps to distinguish smaller peaks from the background, as the counts are concentrated in few channels the produced peak is more pronounced.

The uncertainty in the charge production through the absorption of gamma-rays increases with the energy of the absorbed gamma-ray and therefore the FWHM in the gamma spectrum increases with higher energies. This uncertainty depends on the energy barrier needed to create a charge pair. This energy barrier is much larger for scintillator materials. Within this lies the main reason why scintillator detectors have lower resolution than semiconductor detectors.

The other uncertainty reason of incomplete charge collection in the detector material leads to a low-energy tail. This is because not all the charges are collected (because of losses or a collection delay) which reduces the pulse height produced by the preamplifier and thereby moves counts to the low energy side of the Gaussian peak.

Lastly there is electronic noise which is a constant value and therefore small peaks are affected by it more severely. The most critical part is the detector-preamplifier coupling, because uncertainties created here will be enlarged by the amplifier. One way of reducing the electronic noise is to also cool parts of the pulse processing electronics. Also there is an optimum shaping time for the amplifier at which the electric noise is at a minimum.

Compared to semiconductor detectors the electronic noise is not as important for scintillator detectors, as the charge production uncertainty is very large.

2.7 Calibration of the spectra

So far the spectrum is only the counted amount of electric signals against number of channels. By calibrating it, the gamma-ray spectrum is transferred into a depiction of counts against energy. Additionally to this energy calibration, the peak width and the efficiency have to be calibrated to enable a correct interpretation of the peaks regarding the kind and amount of isotopes present. This calibrations are done using gamma-ray spectra that are carefully measured with prepared special samples of known isotope composition and concentration.

2.7.1 Energy calibration

The energy calibration provides the relation between the channel number and the energy. Therefore the peaks in the spectrum can be associated with the energy of the gamma-ray that caused them. The calibration is done by comparing the measured peaks from the known source, containing one or more kinds of isotopes, with their well-known energies. The used calibration peaks should cover the entire energy range in which the spectrum is going to be used. This creates an energy to channel relationship that represents the energy calibration. If the spectrum has no energy calibration whatsoever, the first energy calibration possible has to be done by hand, before a program can do a more precise calibration based on the energy to channel list. Usually a two point energy calibration is sufficient, as the energy to channel relation should be approximately linear.

2.7.2 Peak width calibration

Provides the relation between peak width (FWHM) and the energy. The approach is the same as for the energy calibration and can be done simultaneously. Again there is an approximately linear correlation between FWHM and channel number (now already energy). But the relation shows more scattering than the energy to channel, as FWHM values have a greater inherent uncertainty. The calibration is necessary if a computer program is included in the analysis of the spectrum. Since the FWHM of the peak is estimated by an algorithm the uncertainty in FWHM also greatly depends on the measured peak being well defined. Since the 511 keV annihilation peak and single escape peaks are wider because of Doppler broadening, they should not be used for calibrations.

2.7.3 Efficiency calibration

Provides the relation between number of counts from the detector and the real disintegration rate. The relation of efficiency to energy is given by the absolute full energy peak efficiency, which relates the peak area in the measured spectrum to the radioactivity amount present in the sample. Therefore the production date of the sample must be given, to account for activity reduction from radioactive decay. To gain the efficiency curve, many gamma-ray peaks are measured and their efficiency is plotted against energy. For p-type detectors the efficiency falls for low energy (<130 keV) because of absorption in the detector cap and the dead layer. N-type detectors and planar detectors are more linear and horizontal for the low energy spectrum region.

To derive an equation for the efficiency calibration the curve is divided into two regions at the high point of about 130 keV. Again the 511 keV annihilation peak can be problematic because of its increased width. This efficiency calibration can now be applied to the measured spectra. If the samples are measured against a reference taken with the same setup the efficiency calibration is not needed.

3 Detectors

To have sufficiently high absorption coefficients for gamma radiation the detector materials are solid. The absorbed gamma-rays excite electrons in the detector material, which ionizes and excites the atoms in the material, creating electron-hole pairs. The number of produced electron-hole pairs is proportional to the energy of the gamma-ray. These electrons and holes are then collected by the detector and generate the electrical signal.

3.1 Semiconductor detectors / High Purity Germanium detectors (HPGe)[2]

The basis of the semiconductor detector type is the charge collection by an electrical field that sweeps the charge carrier out of the detector material. The absorbed gamma-rays produced these electron-hole pairs in the detector material. To keep the detector size low and still have complete absorption, a high atomic number of the material is desirable, as this increases the absorption coefficient.

Semiconductor materials have a full valence band and a band gap to the conduction band that is in the order of 1 eV. This is an energy amount that can come from thermal excitation, therefore a small amount of electrons will always be present and the material will have a certain amount of conductivity. As this effect strongly relates to temperature, semiconductor detectors are cooled to reduce this so called leakage current. Through this reduction of background current the extra excitations from gamma-ray interactions are detectable. Every electron that is moved into the conduction band will also create a hole in its original band, which is an additional charge carrier and contributes to the conductivity of the material. Since the excitation energy of gamma-rays is significantly higher than the thermal excitation, also electrons from deeper bands can reach the conduction band and even reach energy levels well above the start of the conduction band. Nevertheless the electrons will migrate to the base of the conduction band and the holes to the top of the valance band through cascade processes. The produced number of electron-hole pairs is directly related to the energy of the gamma-ray and depends on the energy needed to create the electron-hole pair for the used material. The energy needed to create an electron-hole pairs should ideally be rather low. Also the material must satisfy certain criteria to enable a high mobility of the charge carriers so that they can be collected in a short amount

[2] The Practical Gamma-ray Spectrometry (Gilmore, 2008) and Germanium Detectors (Canberra Industries, 2014).

of time at the collection contacts. This is gained by a high purity of the material and perfect crystal structure.

The material fulfilling these demands best is Germanium, nevertheless it needs to be cooled by liquid Nitrogen to 77 Kelvin to reduce the otherwise too dominant leakage current. The needed low temperature also increases the mobility of the charge carriers. Although there are other possible semiconductor materials that have a higher atomic number (larger absorption coefficient) and a bigger band gap (fewer thermal excitations), their properties regarding crystalline perfection and charge carrier mobility limit their use. They are mostly used when space is limited and no Nitrogen cooling is possible.

A detector consist of two regions of Germanium - p- and n-type. The p-type is doped with materials that only have three valence electrons - this acceptor impurity produces holes, thereby creating additional energy states above the valance band. The n-type is doped with materials that have five valence electrons (donor impurities), which produce additional energy states below the conduction band. At the contact zone of the two regions the excess electrons and holes annihilate, and a charge depleted layer is created, creating a contact potential across the depleted layer. This depletion layer is the active element of the detector and therefore should be as big as possible. To produce such a structure, a block of high-purity Germanium is created, either n- or p- doped, and a layer of opposite doping as added to one side. Now a reverse bias is applied which extends the depleted layer throughout the entire material. The electron-hole pairs, which are produced in this layer by absorbed gamma-rays, are swept to the electrodes by the electric field and their charge is converted into a voltage pulse by a preamplifier. There are several different shapes the detector crystal can have, these are shown in Figure 3 together with their efficiency over the energy spectrum.

HPGe detectors are mounted in a cryostat to keep them at 77 K and to isolate them from mechanical vibrations. Also they must be contained in a clean vacuum to prevent condensation on the detector. The detector cap must withstand the vacuum but still allow the gamma radiation to pass through it and reach the detector. A schematic of a possible HPGe detector setup with liquid Nitrogen reservoir can be seen in Figure 4.

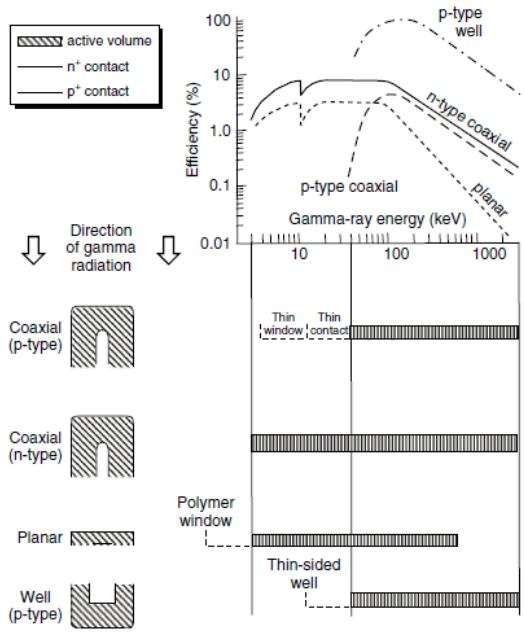

Figure 3 Possible detector configurations, their efficiency curves and the energy range in which they might be used (Gilmore, 2008).

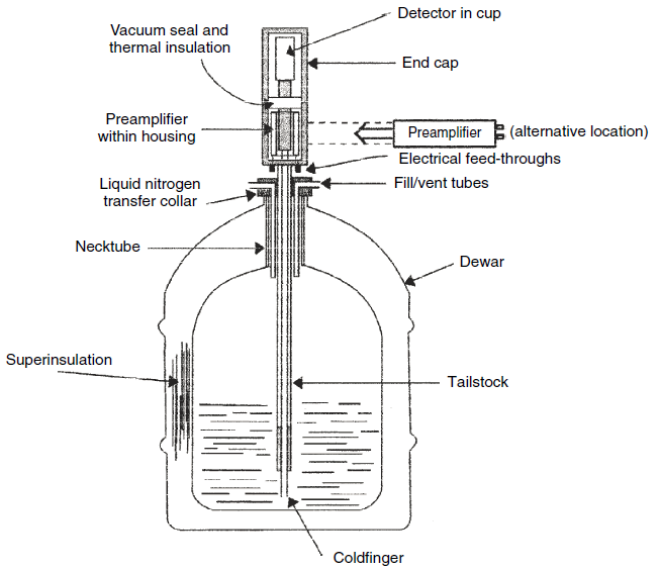

Figure 4 Schematic of Germanium detector inside a cryostat with a liquid Nitrogen reservoir (Gilmore, 2008).

3.1.1 Broad energy Germanium detector (BEGe)[3]

The specific detector used for the measurements was the Be5030 model from Canberra Industries. A detailed overview of the specifics is given in Table 1. The energy range of the detector covers the range of 3 keV to 3 MeV with an efficiency and energy resolution optimization of the energy region of 3 to 662 keV, that is equivalent to that of a low energy Germanium detector. The detector has a short, fat shape to gain this enhanced efficiency below 1 MeV. This makes the detector also more transparent to high energy cosmogenic background radiation and high energy gammas from naturally occurring radioisotopes and therefore lowers the recorded background. Since the detector is stationed above ground in a structure on top of the Vienna International Centre, the lower background from cosmogenic radiation is of particular advantage.

The detector has an electrode structure that enhances low energy resolution, and the impurity profile of the Germanium crystal improves charge collection which increases resolution and peak shape.

[3] This chapter is based on the following documents of Canberra Industries (Detector Specification and Performance Data, 2011; Detector Specification and Performance Data After Repair, 2014; Broad Energy Germanium Detectors (BEGe), 2013).

Active Area [mm²]	Thickness/ Length [mm]	FWHM resolution at given energy			Endcap diameter [mm (In.)]
		5.9 keV (Fe-55)	122 keV (Co-57)	1332 keV (Co-60)	
5000	30.5	0.465	0.683	1.705	102 (4.0)

Table 1 The given values differ from the standard configuration of this model as they were changed during repair work. The values of the FWHM resolution are not the guaranteed maximum values of this detector model, but the measured values for this specific detector; measured by Canberra prior to the return after the repair work.

The window material is Carbon Epoxy with a thickness of 0.6 mm and it is 6.4 mm above the crystal. Carbon windows are robust and have good transmission to below 10 keV.

Apart from the detector the preamplifier was a 2002CSL model and the Cryostat a 7500SL-RDC-4-ULB model.

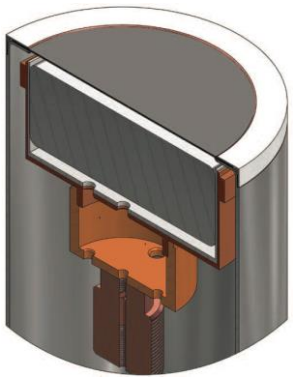

Figure 5 Schematic of the BEGe detector model from Canberra (Canberra Industries Inc., 2013).

3.2 Scintillator detectors[4]

Bevor the commercial development of semiconductor detectors, scintillator detectors were the main standard in gamma spectrometry. This is reflected in the fact that the description of detector efficiency is still described in reference to the Sodium Iodide detector. Although semiconductor detectors have advantages for spectrometry of many gamma-rays, scintillator detectors are favourable in hostile environments or in limited space. This is especially so after the development of new scintillator detectors like Lanthanum based detectors.

Scintillators are isolators and the process of generating a signal from gamma-rays differs from the one used in semiconductors. The gamma-ray again produces primary electrons which produce electron-hole pairs. However the secondary electrons cannot be raised high enough to reach the conduction band. The electron and the electron hole stay

[4] This chapter is based on Practical Gamma-ray Spectrometry (Gilmore, 2008).

electrostatically attracted and form a so called exciton. The electron is elevated to an extra band slightly below the conduction band. The electrons can then de-excite and fall back to the holes in the valence band, emitting electromagnetic radiation. This radiation can be collected by photomultipliers or other light measuring devices to produce a detector signal. Scintillators for gamma spectroscopy must fulfil certain properties:

- The material should have a high density and atomic number to provide a high stopping power for gamma rays.
- The production of electron-hole pairs must be high enough per unit of gamma-ray energy.
- The response must be proportional to the energy of the gamma-ray and, to enable high count rates, the decay time of the excited state must be short.
- Furthermore the scintillator material must be transparent to the produced light.

To gain these properties an activator is needed, introducing a small amount of impurities. The impurities create additional levels in the forbidden zone between the continuum band and the valence band. The ground state of the activator band is above the valence band and can be populated by the holes. The excited states of the activator lie below the conduction band and can be reached by the electrons. The de-excitation will now produce photons with longer wavelength which should be in the visible range. This also causes the emitted wavelength to no longer be in the absorption region of the scintillator. Nevertheless not all absorbed gamma-ray energy will be re-emitted as light, some is converted in lattice vibrations or heat. The NaI(TI) crystal has a light output of about 12% of the total incoming gamma radiation.
The lifetime of the excited activator state is only of the order of 0.1 µs. This direct emission is called luminescence and enables very short detector pulses. Although most of the time only one excited state is significantly populated, there are also other more complex decay events. The direct transition to the ground state is forbidden for some of the excited states, leading to a more complex de-excitation and a slower decay of the emitted light. This afterglow increases the background to the next pulses.

The major advantage of scintillation detectors over HPGe detectors is that they can be operated at room temperature, with some materials even having their maximum light

output there. Although the light output is stable in the region of room temperature, it decreases if the temperature gets too high or low.

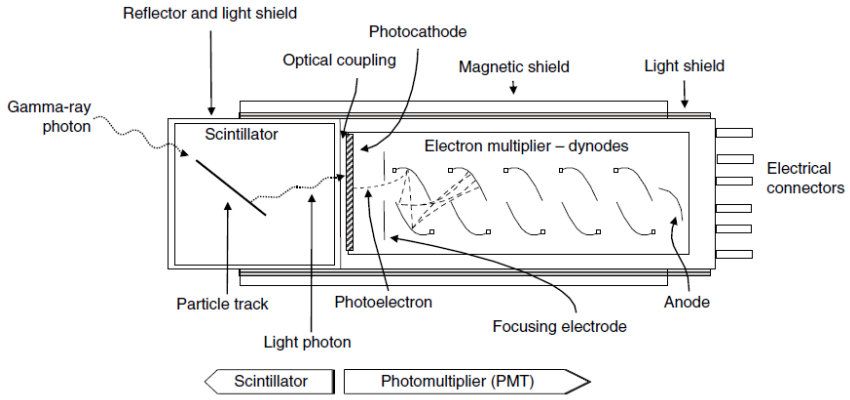

Figure 6 The photons from the scintillator pass through the optical coupler into the photomultiplier at which end the amplified signal is passed to the measurement circuits (Gilmore, 2008).

The light output of the scintillator is enhanced and converted into an electrical signal via a photomultiplier. The light from the scintillator hits the photocathode which in turn emits photoelectrons. As the scintillator emits light in all directions, it is surrounded by reflectors to increase the amount of light reaching the photocathode. Since most scintillators are hygroscopic they have to be hermetically sealed to avoid damage. The energy of the scintillator photons is very low therefore only a small amount of electrons manage to leave the surface of the photocathode. Overall about 100 eV of gamma-ray energy are necessary to produce one primary electron at the photocathode. The produced electrons are then multiplied in a series of dynodes. Because the path of the electrons between the dynodes can be affected by magnetic fields the photomultiplier is surrounded by a magnetic shield. The amplified signal is collected at the anode and passed to the preamplifier.

The FWHM values (resolution) of scintillator detectors are much higher than those of semiconductors. The scintillator resolution is conventionally given as a calculated percentage of the peak energy: $W = FWHM * 100 / E$. Although this means that the resolution value W will increase with increasing energy, the peaks still become progressively broader with higher energies.

The width of the peak (ergo the resolution) depends on three groups of uncertainties. Primarily it depends on the statistical uncertainties within the production of the signal, such as produced electron-hole pairs, the number of photoelectrons that escape the photocathode and the signal multiplication in the electron multiplier. These are the most

dominant sources of line broadening. Secondly, non-linear effects occur in the conversion of the gamma-ray energy into light by the scintillator. This term has the biggest impact on width changes and is a function of the gamma-ray energy. The third factors derive from the overall characteristics of the detector system, such as the purity of the detector material or the coupling of the light into the photomultiplier.

There are several differences regarding the demands on the electronics for scintillator detectors compared to semiconductor detectors. For one the high-voltage supply needs to provide a greater current for the bias supply of the photomultiplier. Also the stability is more important, to provide a stable signal gain in the photomultiplier.
Contrary to the semiconductor detectors the electronic noise is not a problem and therefore the preamplifier, which integrates the current pulses coming from the photomultiplier into a signal, does not need low noise specifications. The same applies for the amplifier. The rise time of scintillator pulses are faster, therefore the time constants are in the range of 0.2 – 3 µs. Also there are no special strains on the MCAs, because of the low resolution of scintillators, compared to semiconductor detectors, the needed number of channels is also lower.

Recently some new scintillator materials have been developed decreasing the disadvantages such as: brittleness, sensitivity to temperature changes and long afterglow. One of which is the material combination of Lanthanum Bromide.

3.2.1 Lanthanum Bromide detector $LaBr_3$ (Ce)[5]

Lanthanum Bromide with cerium as activator is a new material, used to produce Lanthanum-based scintillators since 2007. A disadvantage of this material is its content of radioactive Lanthanium-138 (La-138) which decays inside the detector and produces an unavoidable background. Because the decay of La-138 happens inside the detector, the full-energy peaks are all summed with other background processes, which increases the respective background peaks in the spectrum.

The specific detector used for the measurements was the BrilLanCe^{TM}380 from Saint-Gobain. The LaBr3 (Ce) crystal is a transparent scintillator material with increased light output

[5] This chapter is based on “Practical Gamma-ray Spectrometry” (Gilmore, 2008) and documents from Saint-Gobain Ceramics & Plastics “BrilLanCe 380 Data Sheet” (Saint-Gobain Ceramics & Plastics, 2014) and “SGC BrilLanCe Scintillator Performance Summary” (Saint-Gobain Ceramics & Plastics, 2009).

emission rate and energy resolution compared to NaI(Tl). The characteristics of the crystal as described in the white paper and the Performance Summary on the Saint-Gobain homepage are the following:

The FWHM for 2”x 2” and a 1”x 1” crystal is given as 2.6% and 2.8% and is expected to lie between these two values for our used crystal size of 1.5”x 1.5”. The emission of scintillation light is between 325 nm and 430 nm, with a maximum at 380 nm, and therefore in the range of standard photomultiplier tubes. The temperature dependence of the detector measured with Cs-137 shows that the light output between 0°C and +55°C changes by less than 1% and by less than 5% in the total range of -65°C to +140°C. The light output at 25°C is 160% of NaI(Tl). The absorption efficiency for the energies of the nuclides of interest for this study can be found in Figure 7. The main peaks of these nuclides are in the energy region of 352 to 537 keV, for which the detector crystal (1.5” or 38mm) has an absorption efficiency between 80 and 90 percent.

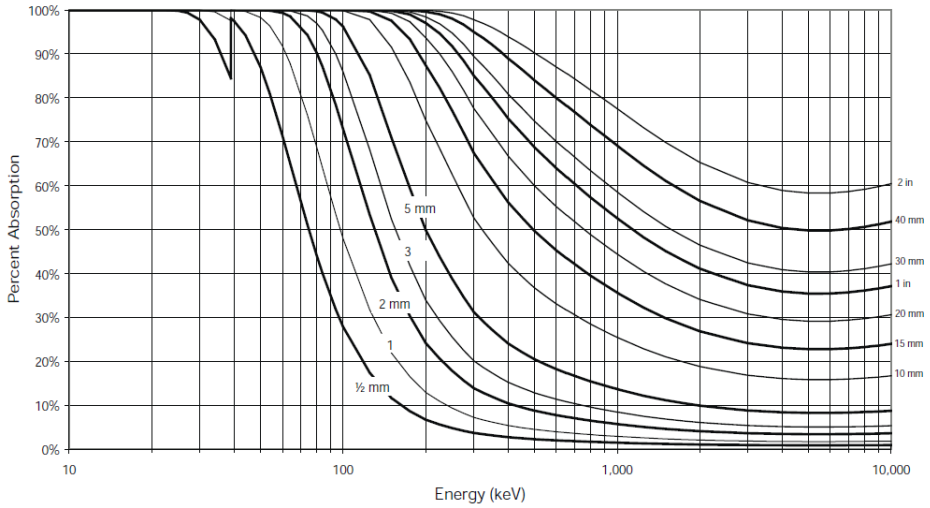

Figure 7 Absorption efficiency of the BrilLanCe 380 detector crystal for various thicknesses from “Efficiency Calculations for Selected Scintillators” (Saint-Gobain Ceramics & Plastics, 2014) the diagram was compiled by C. M. Rozsa.

Of special interest are the energy resolution and the background of the detector, as they determine if the Be-7 peak at 477.8 keV can be detected and the I-131 peak at 364.5 can be resolved. The advantages compared to a NaI(Tl) detector regarding energy resolution and relative efficiency can be seen in Table 2.

Energy (keV)	Resolution B380	Resolution Na(Tl)	Relative efficiency
122	6.6%	8.9%	105%
356	3.8%	9.1%	106%
662	2.9%	7.0%	118%
1332	2.1%	5.4%	143%
2615	1.6%	4.5%	165%

Table 2 Comparison of the BrilLanCe 380 detector (3" x 3") to the standard NaI(Tl) detector regarding their energy resolution and the relative efficiency increase of the B380 compared to the NaI(Tl).

The comparison of the two detectors for the 356 keV peak of Ba-133 shows that the better energy resolution leads to significantly better separation of the energy lines around 350 keV. See Figure 8.

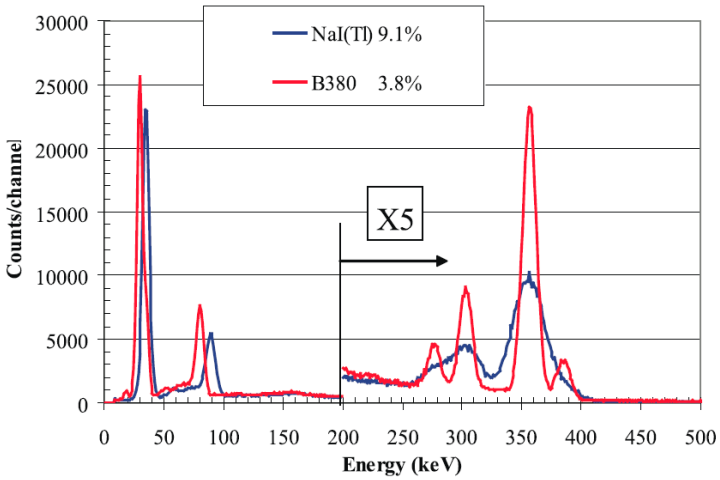

Figure 8 Comparison of the BrilLanCe 380 detector (3"x3") to the NaI(Tl) detector, comparing their energy resolution in the region of 350 keV (Saint-Gobain Ceramics & Plastics, 2009).

Since Lanthanum[6] has the natural occurring radioisotope La-138, which appears with a fraction of 0.09%, there is a certain amount of background in spectra measured with this detector. La-138 decays with a probability of 65.2(6) % via electron capture to Ba-138 and with 34.8% via β^- decay to Ce-138. The Ba-138 is on the first excited level and de-excites by emission of a 1435.816(10) keV gamma photon. The vacancy in the electron shell, produced by the electron capture, leads to a higher shell electron dropping down and emitting an X-ray in the region of 35 keV. (The X-ray energy is most likely at 31.8 keV, with a lower probability up to an energy of 37.4 keV). The Ce-138 de-excites by emitting a 788.744(8) keV gamma. The beta particle, created by the La-138 decay, has an end point energy of 255 keV. A Background spectrum from this crystal, obtained by self-counting can be seen in Figure 9.

[6] The characteristic values for the decay process and the emitted energies are taken from the website of "Laboratoire National Henri Becquerel" (Laboratoire National Henri Bequerel, Recommended Data (by Z), 2015).

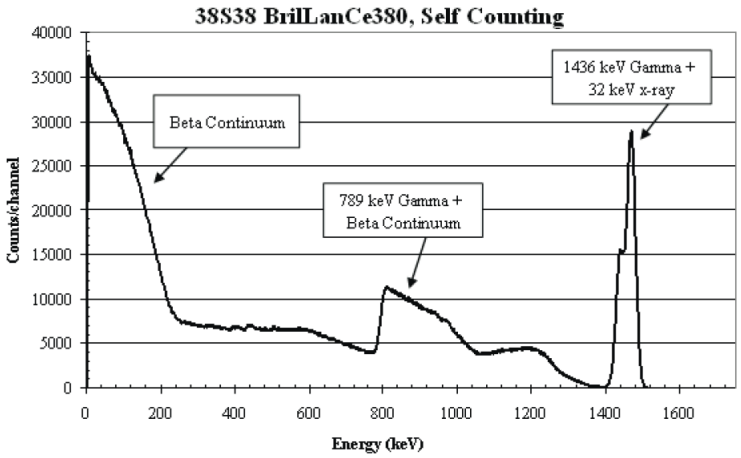

Figure 9 Self-counting background spectrum for a 1.5" x 1.5" detector measured over 3 days (27 878 sec) in a low background chamber (Saint-Gobain Ceramics & Plastics, 2009).

The background spectrum shows the beta-continuum to 255 keV (= Bremsstrahlung). Up to 750 keV there is the Compton continuum from the 789 and the 1436 keV peaks. The 789 keV peak is skewd to a little above 1 MeV, as it is coincident with the beta particle. The 1436 keV peak is shifted to higher energies by the coincident X-ray emission from the shell filling after the electron capture process. This leads to the peak position of about 1473 keV (= summation peak). Above 1750 keV there is some background from a low Ac-227 contamination, but this is low compared to the dominant La-138 peak.

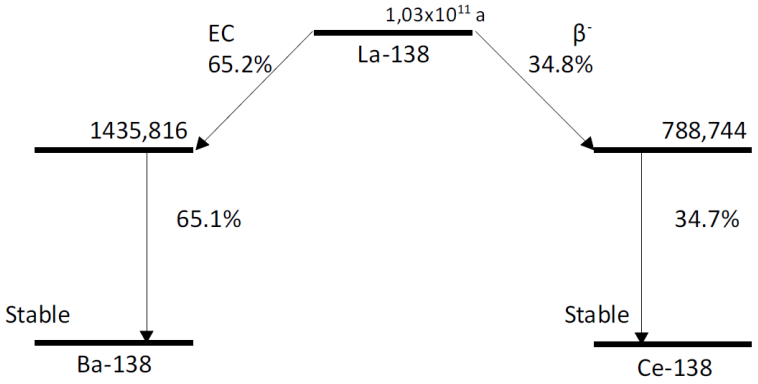

Figure 10 Decay schematic of La-138. The dominant 1436 keV peak can be used as a calibration peak during the operation of the detector (considering that it is shifted to a summation peak of about 1473 keV).

The higher resolution of the BrilLanCe380 allows to distinguish Radon daughters, such as Pb-214 with a peak at 352 keV, from I-131 with its peak at 365 keV, even in complex spectra. Therefore the measured 352 keV peaks are analysed regarding their FWHM.

The described inherent background peak at 1473 keV is used as a calibration peak for the channel shift caused by temperature changes.

4 Characteristics of nuclides of interest

Beryllium 7 is of interest in the LaBr spectra to investigate the sensitivity of the detector, as it is a well examined natural tracer in the atmosphere. The concentration behaviour of Lead 214 is documented in a variety of studies in ground level air (Nagaraja et al., 2003; Pruthvi Rani et al., 2014; Seftelis et al., 2007; Sesana et al., 2003; Papastefanou, 2009). Of special interest in this study is the FWHM of the 351.9 keV peak to asses if the main Iodine peak at 364.5 keV can be distinguished by the LaBr detector. Since the Lead-214 peak is well shaped in the LaBr spectra, it is also of interest to assess the peak shift due to the temperature sensitivity of the detector.

Apart from the sensitivity regarding a temperature shift and the capability to record natural tracers it is also of interest to document the minimal detectable concentration for indicators of fission events. For this purpose the main peak of Iodine-131, at 364.5 keV, and the main peak of Barium-140, at 537.3 keV, have been chosen. They are considered as relevant indicators by the CTBTO for a nuclear explosion, as their detection and concentration differentiate from other sources of radioactivity (CTBTO, 2015).

The characteristic values of the isotopes in this study are all taken from the Webpage of "Laboratoire National Henri Becquerel" (Laboratoire National Henri Bequerel, Recommended Data (by Z), 2015).

4.1 Naturally occurring radioisotopes

4.1.1 Beryllium 7

Beryllium 7 (Be-7) is an unstable isotope of Beryllium with a half-life of 53.22 days. It decays by electron capture into Lithium 7 (Li-7), with 89.56% directly into the ground state of Li-7 or with 10.44% to the excited Li-7 state at 477.6 keV. A graphic depiction of the decay path can be seen in Appendix A. This leads to a yield of 10.44(4) photons per 100 decays for the key line of 477.6035(20) keV (Laboratoire National Henri Bequerel, ^{7}Be, 2004).

The basic processes that determine the production of Be-7 specifically and cosmogenic radioisotopes in general can be found in Physics for Radiation Protection (Martin, 2006) and in Cosmic Ray Produced Radioactivity on the Earth (Lal, 1967). The cosmic radiation, 87% of which are protons, interacts with the components of air to produce neutrons. These secondary neutrons produce several radionuclides such as H-3, Be-7, C-14 or Na-22. The production of the radioisotopes can happen either by spallation or by the capture of thermal

neutrons. The protons of the cosmic radiation themselves produce only a minor fraction of these nuclides.

The variation of the isotopes produced in the atmosphere stem from changes in the cosmic radiation reaching the atmosphere, and the local geomagnetic latitude. The majority of cosmic radiation comes from outside the solar system. Particles from solar flares can increase the amount reaching Earth, but the effects are confined to an increased production rate in the polar region. The main effect of the sun on cosmic radiation reaching Earth comes from the 11 year solar cycle (this also includes the effects of the "forbush type decrease"), solar flares have only little effect. With increasing sun activity, more and more plasma clouds (forbushes) leave the sun, filling an increasing part of the solar system. These plasma clouds represent inhomogeneities of the magnetic field and thereby obstruct the travelling of charged particles, reducing the amount of cosmic radiation reaching Earth. The magnetic fields are only partially opaque to the cosmic particles, especially for the low energy part of the galactic primary particles. This leads to a concentration reduction of radioisotopes, caused by a reduced flux of cosmic rays, in anti-correlation with the sun spot number. Low sun activity creates nearly no travelling clouds of plasma. The effects on the isotope production are especially high at the uppermost regions in the atmosphere and the areas at the poles. The production rate in the troposphere stays nearly unchanged over the course of a solar cycle, even at high latitudes. This behaviour is well documented for tracers such as Be-7 (Cannizzaro et al., 2004; Kulan et al., 2006; Masarik et al., 1999; Steinmann et al., 2013).

Be-7 is produced from the interaction of Oxygen and Nitrogen with the cosmic radiation and to some extent from Carbon. Shortly after Be-7 is produced by the cosmic radiation, it attaches itself to aerosols and therefore travels with the air flow. Upon reaching the lower troposphere it is removed by wet deposition and to a minor amount also by dry deposition. However dry deposition can become important for the case of bomb fall-out. The production rate per cubic centimetre air and second for Be-7 atoms is about 2.7×10^{-2} cm^{-3} s^{-1} in the troposphere and 5.4×10^{-2} cm^{-3} s^{-1} in the stratosphere on a global average. Because of the higher intensity of cosmic rays, about two thirds are produced in the stratosphere; the remaining one third is produced in the troposphere, mostly in the upper regions. This value derives from an averaging over the whole globe. In the stratosphere, the production rate increases from the equator towards the poles. Whereas in the troposphere it is nearly independent from the latitude. The main path of Be-7 from the stratosphere into the

troposphere is convection. In the troposphere Be-7 reaches the cloud bearing layer by dry deposition from where it is removed from the atmosphere by precipitation. The concentration of Be-7 in ground level air has a maximum at around 40°N latitude for the northern hemisphere, if pooled data is compared (Kulan et al., 2006; Steinmann et al., 2013). The reason for the maximum at around 40°N are deep stratospheric intrusions that cause a mixing of stratospheric air into lower tropospheric air, which happens predominantly in the Mediterranean region (Steinmann et al., 2013; Stohl et al., 2003). This happens additionally to the normal slow mixing because of convection. Such stratosphere-troposphere exchanges (STE) have a maximum in late spring and a minimum in fall for the northern hemisphere (Stohl et al., 2003; Zanis et al., 2003). Increased convective mixing within the troposphere during summer leads to an overall concentration increase during summer fed by the higher production rate of Be-7 in the upper troposphere (Steinmann et al., 2013). Increased vertical transfer happens because of a thinning of the border layer between stratosphere and troposphere (tropopause) which increases the vertical transfer (Kulan et al., 2006). This correlation between Be-7 concentration and the STE maximum in spring and the increased vertical mixing of ground air with upper-troposphere air during the warmest months was also observed by Cannizzaro et al. (2004). He also recorded a distinct connection between low precipitation and an increased Be-7 concentration of ground level air.

To gain an understanding of the possible values the activity concentration of Be-7 can have, reference values were taken from Steinmann et al. (2013), "Cosmogenic ^{7}Be and ^{22}Na in ground level air in Switzerland". Their measurements were taken at 5 collection sites in Switzerland: Oberschrot (7.3° E, 46.7° N, 1040 m a.s.l.), Monte Ceneri (8.9° E, 46.1° N, 586 m a.s.l.), Güttingen (9.3° E, 47.6° N, 439 m a.s.l.), CERN (6.1° E, 46.2° N, 421 m a.s.l.) and Klingnau (8.2° E, 47.6° N, 318 m a.s.l.). This is a good representation for the degree of latitude for Vienna (48.21° N, 16.37° E), since the Be-7 concentration varies with the degree of latitude as described above. The long term measurement took place between 1994 and 2011, with weekly filter exchanges and measured with an HPGe detector. The monthly pooled average Be-7 concentration of all 5 stations can be seen in Figure 11.

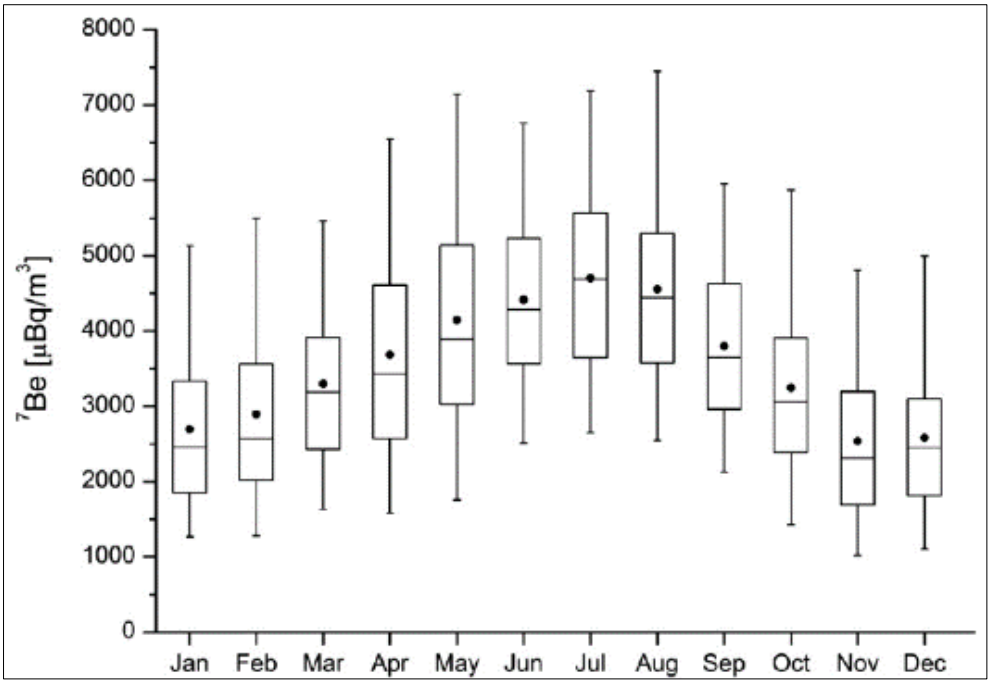

Figure 11 Pooled monthly Be-7 concentration of ground level air, measured in Switzerland by Steinmann et al. (2013).

Another source of reference values to compare our Be-7 concentration results with was taken from Kulan et al., “Distribution of Be-7 in surface air of Europe” (2006). Among others he lists Be-7 concentration for Prague (50.05° N, 14.22° E), which again is geographically close to Vienna. The measured concentration was on average 3109 µBq/m³ with peaks commonly reaching values between 4000 and 7000 µBq/m³. These measurements where done by Rulik et al. (2005), with weekly HPGe detector measurements in the time from 1986 to 1999.

4.1.2 Lead 214

Lead 214 (Pb-214) is an unstable isotope of Lead with a half-life time of 26.916 (44) minutes and decays into different excited states and the ground state of Bismuth 214 (Bi-214). The Bi-214 state with the highest photon yield is 351.932(2) keV with 35.60(7) photons per 100 decays, followed by 295.224(2) keV with 18.414(36) photons per 100 decay (Laboratoire National Henri Bequerel, ^{214}Pb, 2010). A detailed graphic overview of the decay scheme can be found in Appendix A.

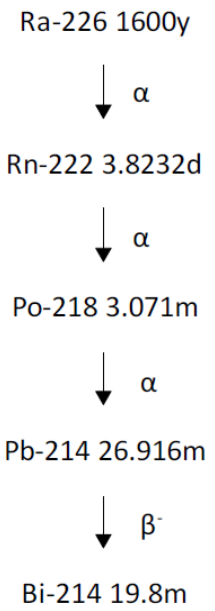

Figure 12 Radioactive serious from Ra-226 to Bi-214.

Pb-214 is a radionuclide from the natural decay chain of U-238. It is a short-lived daughter of Radon 222 (Rn-222) which has a half-life of 3.823 days. Rn-222 decays into Po-218 which has a half-life of 3 minutes and further decays into Pb-214. Rn-222 is the first gaseous decay product and therefore diffuses from the ground into the atmosphere. It appears in all soils and minerals in varying concentrations. As the precursors of Rn-222, U-238 (4.5 billion years), Th-230 (75 380 years) and Ra-226 (1600 years) are in equilibrium in the soil, it has a constant natural source. Pb-214 is again a solid particle and, because of its electrical charge, attaches to dust particles (Martin, 2006).

Because the short half-life of Pb-214 (26.916 min) compared to that of Rn-222 (3.823 days), it is in secular equilibrium with its parent and therefore the variations of Pb-214 follow those of Rn-222. The concentration of Rn-222 in the atmosphere near the ground and its release rate from the ground depends on geological and weather factors such as temperature, humidity, wind speed and the composition of the ground (Pruthvi Rani et al., 2014; Seftelis et al., 2007).

The typical diurnal variation of Rn-222 on a day with low wind speed (<4 m/s) and no precipitation shows the following pattern (Nagaraja et al., 2003; Pruthvi Rani et al., 2014; Seftelis et al., 2007; Sesana et al., 2003): A peak in the early morning followed by a decline until it reaches a minimum in the afternoon then an increase to a second smaller peak in the evening followed by the incline to the maximum of the next morning.

This variation derives from the different factors that affect the Radon concentration:

1. Reduction of Radon concentration caused by warming the air near the surface (Nagaraja et al., 2003; Seftelis et al., 2007; Sesana et al., 2003). Air warmed by the sun leads to an upwards air flow, pushing the Radon in higher layers of the atmosphere. The sun heats the air during daytime, inducing turbulences which transport Radon faster upwards (Seftelis et al., 2007).
2. The temperature inversion (higher air layers are warmer then the lower ones), often present during night time and in the early morning, especially in combination with low wind, traps the Radon near the ground and increases the

concentration (Nagaraja et al., 2003; Pruthvi Rani et al., 2014; Seftelis et al., 2007; Sesana et al., 2003).

3. Through rainy periods the aerosols are removed and washed into the soil. This leads to reduction of the Radon concentration. Although the overall concentration is lowered, the diurnal variation is still present (Nagaraja et al., 2003; Seftelis et al., 2007).

These points lead to a similar diurnal variation during winter, summer and rainy periods for Radon and its daughter products. The concentration is on its maximum during winter, in rainy periods it is slightly reduced and the concentration is minimal during summer (Nagaraja et al., 2003; Pruthvi Rani et al., 2014; Sesana et al., 2003).

Apart from nuclear decay the concentration of Radon daughters is also reduced by two further processes. For one dry deposition of the aerosols or, more important, through wet deposition by rain (Papastefanou, 2009).

4.2 Man-made radio isotopes

The amount of radioactive material that is set free by a nuclear explosion is difficult to predict. It depends on several factors such as meteorological conditions (e.g. wind speed and direction), the design of the weapon and its content, the characteristics of the surface underneath the explosion and height above the explosion (Atomicarchive, 2015).
Klement (1953) presents in their report a fission yield for the production of this nuclides in a nuclear weapon explosion of 1 per 10000 fissions for I-131 and 54 per 10000 fissions for Ba-140. They derive these values from data for slow neutrons, which should deviate from the actual values only by a factor of two.
I-131 and Ba-140 are of biological interest regarding hazards to humans in the short and intermediate time frame after the detonation. Particularly because Ba-140 has an internal deposition as it is bone seeking and therefore affects the blood-forming organs and bones. I-131 has similar characteristics, as it is selectively incorporated by the thyroid (Klement, 1959).

4.2.1 Iodine 131

Naturally only the stable isotope Iodine 127 and the radioactive isotope Iodine 129 occur. Iodine 131 (I-131) is a man-made radioactive isotope which is used in medical applications as

a tracer for imaging and thyroid cancer treatment (U.S. Department of Health and Human Services, Toxicological Profile for Iodine, 2004).
Iodine 131 is an unstable isotope with a half-life of 8.0233 (19) days, that decays through β^- emission into Xenon 131 (Xe-131). It mainly disintegrates into the excited level of 364.489 (5) keV, providing 81.2(5) photons per 100 disintegrations (Laboratoire National Henri Bequerel, ^{131}I, 2014). For a detailed view of the decay scheme see the graphic in Appendix A.

The U.S. Department of Health and Human Services states about I-131 in its report on the Toxicological Profile for Iodine (2004): Ingestion of I-131 leads to a concentration in the thyroid where, in its stable form, it is needed to form hormones. But the radioactive isotope leads to damage in the thyroid gland and an increased risk of getting thyroid cancer. I-131 is released into the atmosphere during the normal operation of a nuclear power plant. On average 7-20x10^7 Bq per MW(e)y for BWRs and 2-20x10^6 Bq per MW(e)y for PWRs. However it is released in a higher quantity in case of the use or testing of nuclear weapons and from accidents in nuclear power plants, such as Chernobyl or Windscale (U.S. Department of Health and Human Services, Toxicological Profile for Iodine, 2004).
Masson et al. (2011) investigated the airborne radionuclides over Europe after the damage of the Fukushima Dai-Ichi nuclear reactor and measured the I-131 concentration in the air. The release started on the 12th of March 2011 and the first detections of I-131 in Europe where recorded on 19th of March 2011. In the time period of one month until mid-April peak values reached 1 to 6 mBq/m³ over Europe for particles of I-131 and even up to 11 mBq/m³ for gaseous I-131. The values measured in Vienna never exceeded 2 mBq/m³. However after the Chernobyl accident in 1986 the I-131 values in the air were 3 - 4 orders of magnitude higher (Masson et al., 2011).

I-131 is a major fission product of Uranium and Plutonium. The fission yield of I-131 is about 3% (Wilson, 1966), a more detailed breakdown of the fission yield can be seen in Table 3.

Nuclide	Thermal Fission Yield [% per fission]	Fast Fission Yield [% per fission]	14-MeV Fission Yield [% per fission]
Th-232	-	1.513 ± 0.083	2.31 ± 0.14
U-233	3.565 ± 0.1	3.86 ± 0.13	4.47 ± 0.94
U-235	2.878 ± 0.032	3.365 ± 0.054	4.11 ± 0.14
U-238	-	3.321 ± 0.083	3.62 ± 0.17
Pu-239	3.724 ± 0.078	4.09 ± 0.12	-
Pu-241	3.076 ± 0.074	3.164 ± 0.085	-

Table 3 Cumulative fission yield for I-131, as listed on the IAEA webpage for Safeguards Data (IAEA, 2015).

Therefore its presence in air can be used as an indicator for nuclear weapon tests or the accidental release of nuclear material from nuclear power plants. The knowledge of increased I-131 values in the air is also important to enable protection measures for the general population.

4.2.2 Barium 140

Barium 140 (Ba-140) is an unstable isotope of Barium that decays into various excited levels of Lanthanum 140 (La-140) by β^- emission. It has a half-life of 12.753(d) days. The most dominant transition is to the 537.303 (6) keV excited state of La-140, with 24.39 (22) photons per 100 disintegrations. (Laboratoire National Henri Bequerel, ^{140}Ba, 2008). For a detailed overview of the decay scheme see the graphic in Appendix A.

The U.S. Department of Health and Human Services states about Barium in its report on the Toxicological Profile for Barium and Barium Compounds (2007): Natural Barium exists in many compounds, but is generally in solid form and has many different applications in the industry. The intake of Barium proposes only a health risk if it is in large quantities and in a compound that is soluble in water. Reported effects of high concentrations of Barium in air on humans range from muscle weakness and electrocardiogram abnormalities to nausea and vomiting. Also Barium is determined as not likely to be carcinogenic after intake by the EPA (United States Environmental Protection Agency). However there are no studies conducted regarding the carcinogenic effects from inhalation exposure (U.S. Department of Health and Human Services, Toxicological Profile for Barium and Barium Compounds, 2007).

Of all Barium isotopes produced by fission, Ba-140 is the most important as it has the longest half-life. The half-life of the other Barium isotopes produced by fission is of the order of

seconds or minutes. In the first 10 days after an explosion about 10% of the total activity of the fission products comes from Ba-140 (French, 1963). A detailed breakdown of the fission yield can be seen in Table 4:

Nuclide	Thermal Fission Yield [% per fission]	Fast Fission Yield [% per fission]	14-Mev Fission Yield [% per fission]
Th-232	-	7.71 ± 0.25	5.69 ± 0.2
U-233	6.43 ± 0.26	6.17 ± 0.2	4.47 ± 0.32
U-235	6.314 ± 0.095	5.959 ± 0.048	4.474 ± 0.081
U-238	-	5.972 ± 0.084	4.619 ± 0.037
Pu-239	5.322 ± 0.059	5.303 ± 0.074	-
Pu-241	5.76 ± 0.11	5.36 ± 0.14	-

Table 4 Cumulative fission yield for Ba-140, as listed on the IAEA webpage for Safeguards Data (IAEA, 2015)

5 Method of measurements

The samples that where analysed were gathered on the roof of the Vienna International Centre (VIC) (48.2° N latitude, 16.4° E longitude, 167m a.s.l.) in Austria at a height of 118m, with an IMS (International Monitoring System) station of the CTBTO that is placed on top of the VIC. The used air sampler was a Snow White JL-900 with an average air flow set to 800 m³ per hour. A schematic of the air sampler is shown in Figure 13. The system is equipped with a meteorological station that can measure wind speed and direction, temperature, relative humidity and rain. But this data was not recorded at the time of the measurements as the weather station was not in operation. Therefore the weather data for the region of Vienna was taken from other sources.

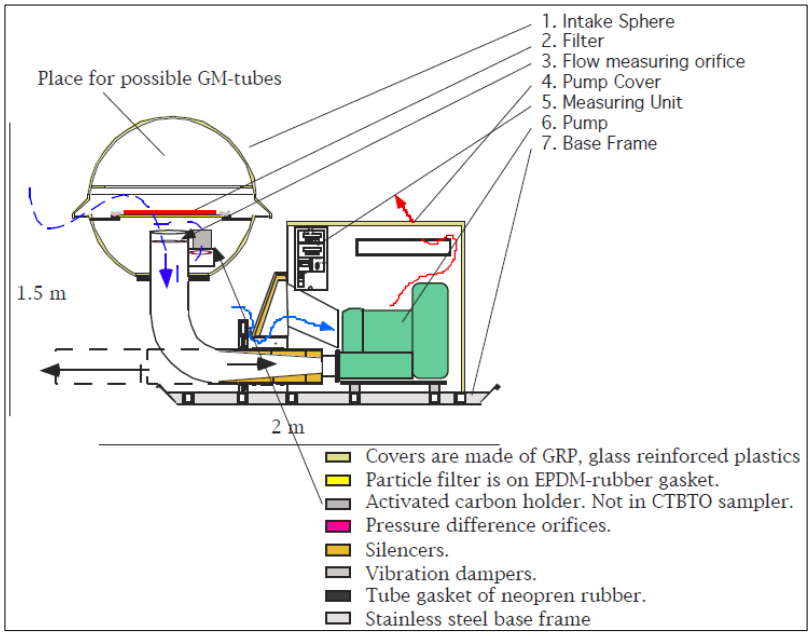

Figure 13 Schematic of the used air sampler Snow White JL-900 (SENYA, 2009). Insted of the possible GM-tube the LaBr detector was mounted in the upper half of the intake sphere.

The LaBr detector is mounted approximately 10 centimetres above the filtering cloth (filter material type 3M) in the upper part of the intake sphere in the place of an optional GM-tube. The detector can be seen if the hood is opened, as shown in Figure 14 and 15. The LaBr detector measures gamma radiation present on the filter during the regular collection time of 24 hours in real time. The measurement times for the gained spectra can be set freely. In this study first a time period of 10 minutes was chosen (leading to 144 spectra during the 24 hours of exposure). These spectra were recorded for the days between 13th of March 2015 and the 19th of March 2015. As the results were not satisfactory the LaBr measurement time was increased to one hour. First a test measurement was done on the 16th of June 2015 to

assess if the spectra gained from one hour measurements provided better outcomes. Since the results were more satisfying, another week long measurement series was taken between the 26th of June 2015 and the 4th of July 2015.

Since the LaBr detector is in the upper intake sphere, its temperature is directed by the environmental temperature, which causes a channel shift. To stabilise the energy calibration against this shift, a program constantly monitors the measured spectra and analyses the position of the multiplet from La-138 and K-40 which have to be at the energy/channels of 1473 and 1441 keV. If the multiplet position changes the program evaluates the channel shift, changes the gain of the amplifier appropriately and also sends the changes to the MCA in order to also adapt the energy calibration. This takes advantages of the otherwise disadvantageous intrinsic background peak from the La-138 portion that is present in the detector material. Therefore the spectra produced by the LaBr detector system are automatically energy calibrated during the measurement process.

Also temperature of the LaBr detector is measured constantly during the measurement process. This data of the detector temperature is also reported by the system and can be used when interpreting the recorded spectra, for example regarding the peak centroid shift or variations of the FWHM of peaks. A detailed description of the implementation of the LaBr detector into the IMS station is given on the poster “LaBr Online Filter Monitoring System: testing results and future project” (Khrustalev et al., 2015).

After the normal exposure time of 24 hours, the air filter is changed and the system is prepared for the next measurement. The used filter is folded and compressed to a disc. Then it is stored in a secure decay box for about 24 hours to allow the sample activity to decay to a lower level before it is measured with the HPGe detector. The measurement time of the HPGe detector is at least 20 hours. This is the standard measurement procedure for certified IMS stations. A detailed list of the specific daily collection, decay and measurement times can be found in chapter 7.1. This leads to a time difference between the results from the two measurement methods of about 50 hours depending on the set length of the single LaBr spectra.

Figure 14 and 15 LaBr detector placement inside the station. If the lid is open the direct placement of the detector above the filter can be seen. (Khrustalev et al., 2015)

6 Method of analysis

The analysis of the spectra that where measured as described above was done with the Genie2000 spectroscopy software of Canberra. The values calculated are: the activity of Pb-214 and activity concentration of Be-7, the MDC of Be-7, I-131 and Ba-140, as well as the peak energy and variation of main peaks of Pb-214 and its FWHM.

6.1 HPGe spectra

To produce a calibration file for the HPGe detector, the spectrum of a long time measurement with a known calibration filter was recorded. This calibration spectrum was then adjusted as follows.

First a peak locate analysis was done with the "Unidentified Second Difference" option using a significance threshold of 3.00 keV and tolerance of 1.00 keV followed by the peak area analysis with the "Sum/Non-Linear Least Squares Fit Peak Area" option, using a fixed tail parameter, a continuum of 1.00 FWHM and a ROI limits determination by the settings of: max. num. FWHMs between peaks of 5.00 keV and max. num. FWHM for left/right limit of 2.00 keV. Following this, the peaks were adjusted using the "Interactive Peak Fit" option to ensure that the residuals are within the 2-sigma border and that the peak is well fitted. The energy calibration was done with the "Energy Full" option from a certificate file, which was created from the certificate shown in Appendix B. The peaks at 59.54 keV and 1836.7 keV where selected by cursor mode and the other peaks entered with the auto function. The used polynomial was of the 2^{nd} order. Before the efficiency calibration, the peak area and peak location analysis was done again and checked, as the efficiency calibration would perform this step on its own otherwise. The efficiency calibration was done with the same calibration file, although the peaks for 255 keV and 320 keV were deleted because of their high deviation. The cross over peak was set to 165.86 keV, the low energy curve was taken of 2^{nd} polynomial order and the high energy curve of 4^{th} polynomial order. This calibration was then stored in a calibration file (CAL-file) to be applied during the analysis of the spectra gained from the exposed air filters.

To analyse the spectra of the air samples an execution sequence was created in Genie2000 consisting of the following steps:

1. Prompt to sample information edit, to load the energy and efficiency calibration from a CAL-file

2. Peak Locate – Unidentified 2nd Diff.

   Significance threshold of 3.00, tolerance of 1.00keV

3. Peak Area – sum / Non-Linear LSQ Fit

   Continuum of 4 channels with a step function, use fixed tail parameter and display ROIs, ROI limits of max. 5.00 FWHMs between peaks and max. 2.00 FWHMs to the left or right

4. Efficiency Correction – Standard

   using the set efficiency calibration type: dual

5. Nuclide Identification – NID w/ Interf. Corr

   The NID library used was the CTBTO-et-Al.nlb. The MDA test was performed and Acq-Time decay correction performed. The tolerance was set to 0.50 keV. The NID confidence threshold was 0.30 and the MDA confidence factor was 5.00%

6. Detection Limits – Currie MDA

   The confidence factor is the same as during the NID, which is 5.00%.

6.2 LaBr spectra

The energy calibration of the detector is done automatically during the measurement of the filter. This has to be done, because the detector is temperature sensitive which shifts the peak channels, as described in section 2.5. The efficiency calibration of the detector already existed and was copied in text-form into the RMS file format of the spectra before they were converted into CNF files. The used efficiency calibration block was gained from the analysis of a 7.50 hour long measurement with a calibration filter by Ileana Radulescu at CTBTO. The gain efficiency block and curve can be seen in Appendix C.

To analyse the spectra created by the LaBr detector the following steps were taken:

- Peak Locate – Unidentified 2nd Diff

  Peak Area – sum / Non-Linear LSQ Fit

  (The specifics for these steps are identical to the ones in the HPGe spectra analysis.)

- Interactive Peak Fit:

  The peak of Be-7 is still too small for the analysis algorithm to identify it automatically. Therefore this peak was inspected manually in every spectrum with the “Interactive Peak Fit” analysis tool. The limits for the region of interest where set to 461 keV and 495 keV (477.8 ± 17), which corresponds to one FWHM interval

around the peak energy in which a high enough peak would have to be found. The expected FWHM of the Be-7 peak was calculated from the FWHM polynomial. Since the FWHM of the 351.9 keV peak of Pb-214 is of interest as well, the fit of this peak was inspected too. Here the region of interest for the Pb-214 peak was set to ±1.5 times the FWHM to ensure the inclusion of the entire peak. The FWHM polynomial states a FWHM of 15 keV for this peak.

- Efficiency Correction – Standard
- Nuclide Identification – NID w/ Interf. Corr
  The NID library used was the CTBTO-et-Al.nlb. The MDA test was performed and Acq-Time decay correction performed. The tolerance was set to 1 FWHM. The NID confidence threshold was 0.30 and the MDA confidence factor was 5.00%
- Detection Limits – Currie MDA

This was followed by another run of the nuclide identification to gain the accumulated activity, by changing the sample information to no build-up, the quantity to 1 and setting the time to the start time of the collection.

The results of interest were displayed in the report section and gathered to be compared and further analysed. During the further analysis of the LaBr results it became apparent that the results gained by this method differ from ones done with a different way of analysis in which the efficiency calibration is applied after the conversion into a CNF file. Further investigation, in cooperation with Ileana Radulescu, showed that, during the conversion into a CNF file, the RMS View rounds the fifth and last digit of the efficiency calibration block that was copied into the file. Since the last digit is not only cut off but rounded this alters the efficiency calibration to an extent that the polynomial for the efficiency curve changes from 3rd order to 5th order. This leads to MDC values that are somewhat higher than with the correct efficiency calibration. Since is not prohibitive in assessing the capabilities of the LaBr detector, the analysis was not redone and the values from the rounded efficiency calibration are shown in the result section. Nevertheless this source of error is significant for more precise measurements with more sensitive detectors and will be looked into further by the corresponding personnel of the CTBTO.

7 Analysis results

The first measurement was done from 12th to the 19th of March 2015. The LaBr detector measurement intervals were set to 10 minutes, followed by the standard HPGe measurement after the filter was removed from the station. But the analysis of the spectra showed that the Be-7 peak could not be found by the LaBr detector for this setup. Furthermore, the shape of the Pb-214 peak was unsatisfactory. Therefore the measurement time of the LaBr detector was increased to one hour. Results from a test measurement on the 16th of June 2015 showed that the Be-7 peak still could not be recorded, although the MDC for Be-7 was reduced by the increased volume of air flowing through the filter. Since the Pb-214 peak was well shaped in this setup, a second measurement was done in the time from the 26th of June until the 4th of July 2015. The results from this measurement are used to compare the sensitivity of the HPGe and the LaBr detector and to analyse the resolution of the LaBr detector regarding the capability to distinguish between the Pb-214 peak at 351.9 keV and the I-131 peak at 364.5 keV.

7.1 HPGe spectra

The HPGe spectra recorded between the 12th and the 19th of March 2015 were taken for the comparison with the 10 minutes spectra recorded by the LaBr detector. The average activity concentration of Be-7 was 3.01E-3 Bq/m³, this correlates very well with the assumed overall values for the latitude of Vienna and for the values recorded by Steinmann (2013). Since the LaBr results for this measurement set were not satisfactory the HPGe results will not be discussed in further depth.

The main measurement took place between the 26th of June and the 4th of July 2015 and were measured by the Be5030 broad energy Germanium detector from Canberra (for specifics see chapter 3.1.1). The results for the concentration of Be-7 and the minimal detectable concentration can be seen in Table 5 and Figure 16. The collection and decay time of the filter as well as the acquisition time of the detector can be seen in Table 6. The particular time intervals differ sometimes strongly from the normal IMS station time setting because of down times during the weekend.

HPGe	Be-7 concn	Be-7 MDC	I-131 MDC	Ba-140 MDC
26.6 - 29.6	5.85E-03	6.81E-06	1.55E-06	4.92E-06
29.6 - 30.6	6.37E-03	1.95E-05	4.02E-06	1.41E-05
30.6 - 1.7	7.17E-03	2.18E-05	4.49E-06	1.57E-05
1.7 - 2.7	6.04E-03	2.13E-05	4.35E-06	1.52E-05
2.7 - 3.7	5.99E-03	2.17E-05	4.53E-06	1.61E-05
3.7 - 4.7	5.96E-03	1.33E-05	2.98E-06	9.75E-06
Min	5.85E-03	6.81E-06	1.55E-06	4.92E-06
Max	7.17E-03	2.18E-05	4.53E-06	1.61E-05
Av	6.23E-03	1.74E-05	3.65E-06	1.26E-05
Med	6.02E-03	2.04E-05	4.19E-06	1.47E-05

Table 5 Results from the measurements with the HPGe detector, the values are given in Becquerel per m^3. The significantly lower MDC values for the first day (26.6 – 29.6) derive from the longer collection time of this spectrum, see Table 6.

Collect time [h]	Decay time [h]	Acq time [h]
63.1	24.3	23.4
24.0	25.1	23.8
24.0	22.5	23.3
24.4	22.3	23.0
26.2	24.0	21.6
28.6	48.6	23.8

Table 6 The time for collection, decay and acquisition of the individual days may differ significantly from the normally set times, this affects the relation of background to measured peaks and thereby the MDC of the recorded spectra.

The significantly lower MDC values for the first measurement (26.6 - 29.6) result from the longer collection time, as this filter was in the station over the weekend and therefore has more than twice the amount of air flow through the filter. Also depending on the nuclide half-life the concentration present on the filter is higher. This increases the relative peak height compared to the background.

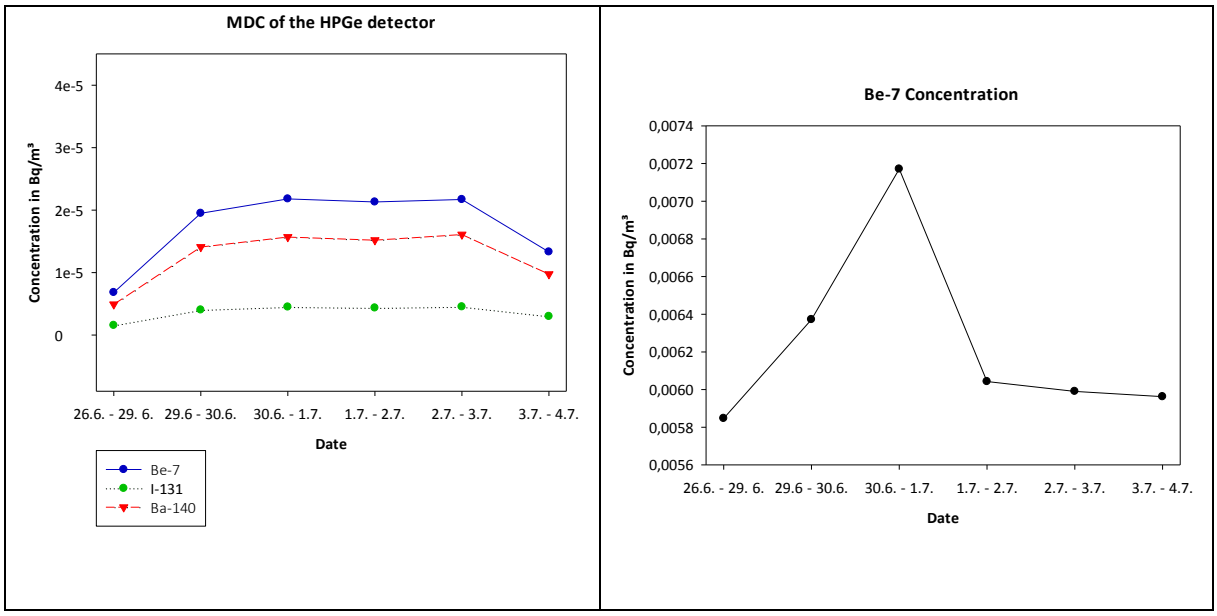

Figure 16 Results of HPGe detector for the MDC of Be-7, I-131 and Ba-140 and the concentration of Be-7.

The slightly lower MDC values for the last measurement (3.7. – 4.7.) derives from the longer decay time between the removal of the filter from the station and the start of the acquisition with the HPGe detector. The longer decay for this filter again originates from the down time over the weekend.

The concentration of Pb-214 was not analysed, because of the long decay period before the filter is measured in the detector most of the lead is already decayed. Even for the minimal occurred decay time of 22.3 hours nearly 50 half-lifes passed for the isotopes deposited last on the filter before the start of the acquisition, reducing the amount of the isotope to just above the MDC limit.

Exemplary spectrum segments showing the Pb-214 peak at 351.9 keV and the Be-7 peak at 477.8 keV can be seen in Appendix E.

The observed concentration of Be-7 is nearly twice the amount as the values that are predicted for the geographical position of Vienna, which is 3500 µBq/m³ (Steinmann et al., 2013) for the annual average value. But there is better agreement with the recorded values for the summer months of June and July by Steinmann (46,1N - 47,6N; 6,1E - 9,3E), with a monthly average of about 4300 µBq/m³ for June and about 4800 µBq/m³ for July. For both months recorded concentrations reach as high as 7000 µBq/m³. The comparison with Be-7 concentrations in Prague, as presented by Kulan et al. (2006), shows a similar situation: The annual average of 3109 µBq/m³ is surpassed by a factor of two, but there are frequent recordings of concentrations reaching up to 7000 µBq/m³.

The detection of such high values is reasonable, if the weather situation of June and July in Vienna is considered. The summer of 2015 was statistically very hot and dry, both characteristics of a weather situation that leads to an increased Be-7 concentration in ground level air. In June the precipitation in Vienna was 55% lower than the average for this month and the average temperature was 1.4 degrees higher. In June higher amounts of precipitation where recorded in Vienna only on the 22nd and 27th at "Wien-Hohe Warte" (ZAMG, Monatsrückblick, 2015). The "Universität für Bodenkultur Wien" recorded higher amounts of precipitation on the 15th, 22nd and 27th (University of Natural Resources and Life Sciences, 2015). The weather situation in July was similar, with exceptionally high temperatures and no precipitation especially in the first half of the month. The precipitation in Vienna was 45% below the average and the average temperature was 3.1°C higher, it was the hottest July ever recorded in Austria. Until the end of measurements on the 6th of July 2015 there was no precipitation in July. This weather situation of lower precipitation and higher than average temperatures affected the entire eastern regions of Austria. (ZAMG, Monatsrückblick, 2015) A reduction in the Be-7 concentration in the air through the recorded precipitation on the 27th of June cannot be seen in the measured data.

Apart from the combination of hot and dry summers, which favours a higher Be-7 concentration, the current amount of sun activity has to be considered. When using the long term average values for Be-7 concentration as a reference, it also has to be mentioned that the solar activity in 2015, although the sun-cycle is currently not at a minimum, is rather low (small number of sun spots) (NASA, 2015; Spaceweatherlive, 2015), therefore the overall Be-7 activity concentration can be assumed to be higher than the given average.

7.2 LaBr spectra

The spectra obtained with a measurement time of 10 minutes show no peak for Be-7, also the Pb-214 peak is not well pronounced. Therefore the detector measurement time was increased to one hour to increase the isotope amount on the filter. But the measured concentrations for Be-7 are still below the MDC limit for the spectra of the one hour measurements. Thus only the results of the last 6 spectra (last 6 hours) before the filter was changed are presented. However the Pb-214 peak was always well defined and was analysed for all spectra recorded in the observation period between the 26th of June and the 7th of July 2015.

7.2.1 Beryllium 7 results

The calculated MDC values of the spectra acquired with the LaBr detector for the one hour measurements can be seen in Table 7 and Figure 30 in Appendix D. The variation of MDC between the different filters is shown in Figure 17, for the last spectrum measured each day. As seen in the results from the HPGe detector the MDC values of the last spectra on the first measurement day are significantly lower because of the longer collection time, which increased the total air flow through the filter.

LaBr MDC values (in Bq/m³)

26.6. - 29.6.	Be-7 MDC	I-131 MDC	Ba-140 MDC
01:30	1.76E-02	2.58E-03	1.24E-02
02:30	1.73E-02	2.59E-03	1.20E-02
03:30	1.79E-02	2.62E-03	1.21E-02
04:30	1.68E-02	2.60E-03	1.20E-02
05:30	1.70E-02	2.59E-03	1.22E-02
06:30	1.68E-02	2.51E-03	1.18E-02

29.6. - 30.6.	Be-7 MDC	I-131 MDC	Ba-140 MDC
04:30	5.67E-02	8.70E-03	3.99E-02
05:30	5.20E-02	8.21E-03	3.85E-02
06:30	5.31E-02	8.22E-03	3.68E-02
07:30	4.49E-02	7.21E-03	3.47E-02
08:30	4.18E-02	6.46E-03	3.27E-02
09:30	4.14E-02	6.09E-03	3.06E-02

30.6. - 1.7.	Be-7 MDC	I-131 MDC	Ba-140 MDC
07:30	6.16E-02	9.68E-03	4.38E-02
08:30	5.55E-02	8.76E-03	4.07E-02
09:30	5.10E-02	7.81E-03	3.61E-02
10:30	4.76E-02	7.27E-03	3.37E-02
11:30	4.32E-02	6.78E-03	3.16E-02
12:30	4.47E-02	6.52E-03	3.02E-02

1.7. - 2.7.	Be-7 MDC	I-131 MDC	Ba-140 MDC
07:30	5.57E-02	8.51E-03	4.06E-02
08:30	5.40E-02	8.13E-03	3.76E-02
09:30	5.06E-02	7.58E-03	3.54E-02
10:30	4.52E-02	7.10E-03	3.34E-02
11:30	4.43E-02	6.79E-03	3.16E-02
12:30	4.30E-02	6.44E-03	3.07E-02

2.7. - 3.7.	Be-7 MDC	I-131 MDC	Ba-140 MDC
07:30	5.86E-02	8.99E-03	4.14E-02
08:30	5.43E-02	8.29E-03	3.89E-02
09:30	5.17E-02	7.73E-03	3.67E-02
10:30	4.79E-02	7.24E-03	3.40E-02
11:30	4.58E-02	6.94E-03	3.39E-02
12:30	4.39E-02	6.57E-03	3.18E-02

3.7. - 4.7.	Be-7 MDC	I-131 MDC	Ba-140 MDC
09:30	5.37E-02	8.16E-03	3.81E-02
10:30	4.95E-02	7.42E-03	3.58E-02
11:30	4.66E-02	6.94E-03	3.32E-02
12:30	4.37E-02	6.74E-03	3.20E-02
13:30	4.28E-02	6.26E-03	3.01E-02
14:30	3.81E-02	6.05E-03	2.91E-02

Table 7 Detailed results of the MDC values for the last 6 spectra/hours of the LaBr detector of each day. The continuous reduction of the MDC level with the increase in collection time / air flow amount is visible.

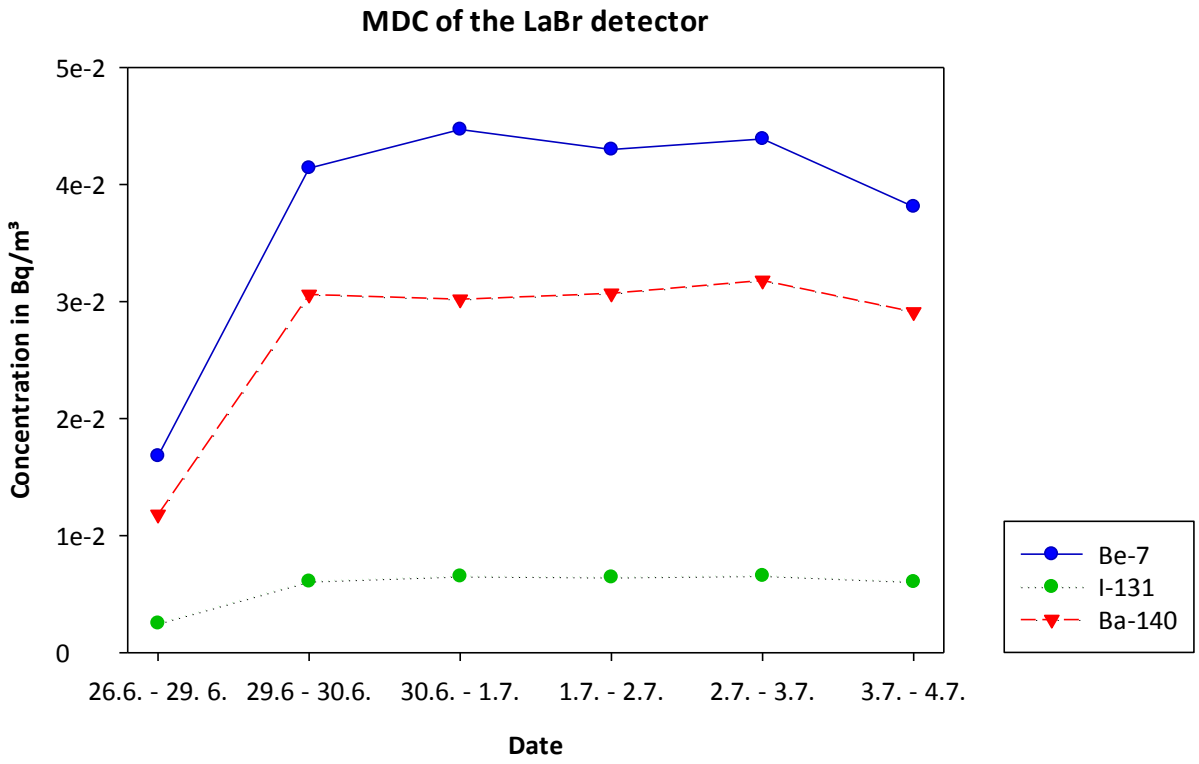

Figure 17 Variation of the MDC between the last LaBr measurement of the different filters. The significantly lower values for the first filter derive from the longer collection time (62 hours) and the therefore higher total air flow through the filter.

It was only possible to fit a Gauss function around 477.8 keV for a small number of spectra and the received concentration was always below the calculated MDC. Therefore the concentration of Be-7 could not be measured. This is illustrated in Figure 18, the spectrum shows the peak of Be-7 taken on the first measurement day one hour before the filter was changed. Since this is the longest deposition time during the entire observation period (62 hours), the concentration of Be-7 on the filter is higher than for the normal filter measurements. The measured activity concentration in this spectrum of 4640 µBq/m³ is under the calculated MDC level (17 000 µBq) of the LaBr detector. One can see that the region in which the Be-7 peak has to be situated, 477.8 ± 1 FWHM, has no distinct peaks. To the right of the supposed Be-7 peak one can see the 511 keV annihilation peak, which is always small but clearly distinguishable. As a comparison the sharp increase in counts on the far left of the Figure 18 highlights the clearly visible Pb-214 peak at 351.9 keV.

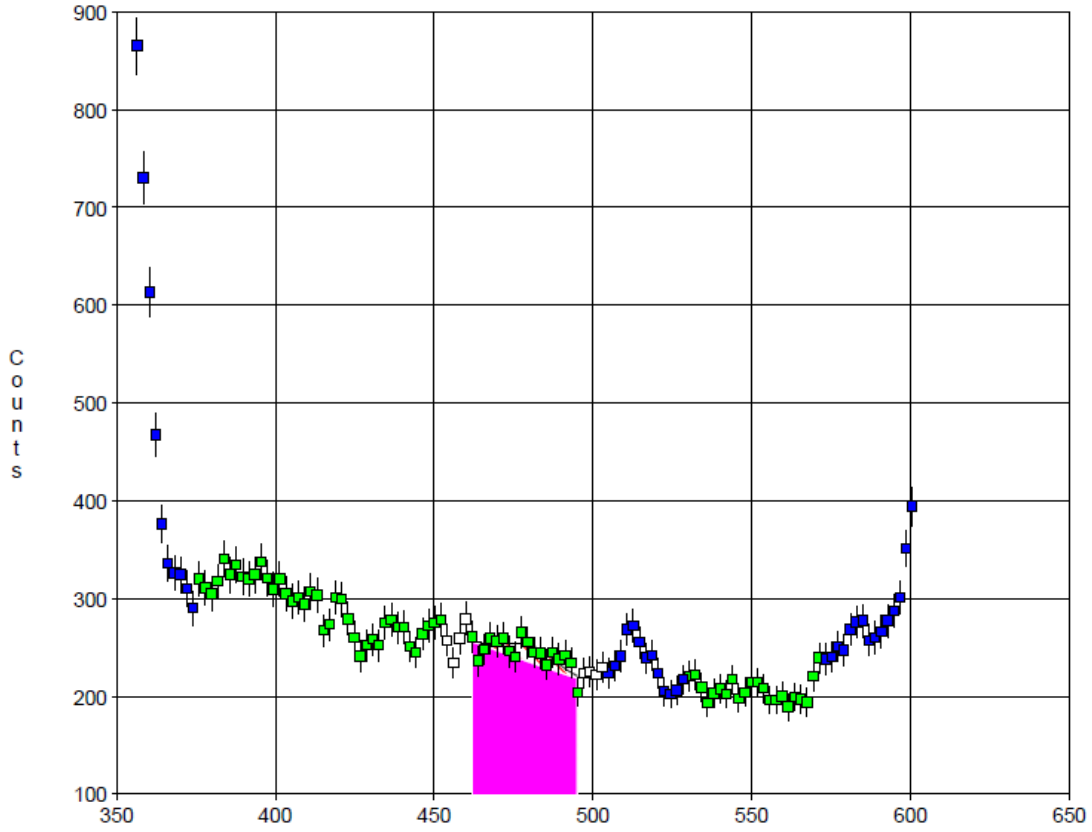

Figure 18 Best recorded 477.8 keV Be-7 peak during the measurements. Although the peak can be fitted and has an activity concentration close to the HPGe results it still is below the MDC level. To the left of the Be-7 peak the 511 keV annihilation peak can be seen, to the right the step count increase of the 351.9 keV peak of Pb-214 is visible.

Results from the 10 minute setup

As a comparison the MDC values, which were calculated from the spectra created during the LaBr measurements with the acquisition time set to 10 minutes, can be seen in Table 8 and Figure 19. The shown values are from the last spectrum recorded before the filter was changed. The MDC is higher because of the shorter acquisition time and because the airflow is only one sixth of that of the one hour measurement. The tip in the MDC values derive again from a longer collection time accompanied by a higher accumulated air flow through the filter over a weekend.

Date	Be-7 MDC	I-131 MDC	Ba-140 MDC	Collection time [h]
12.3. - 13.3.	1.13E-01	1.56E-02	7.68E-02	24.1
13.3. - 16.3.	3.73E-02	5.69E-03	2.81E-02	67.4
17.3. - 18.3.	1.10E-01	1.54E-02	7.54E-02	24.0
18.3. - 19.3.	1.11E-01	1.62E-02	8.34E-02	24.1

Table 8 MDC results in Becquerel per m³ from the last 10 minute measurements of the spectra recorded in March 2015 together with collection time.

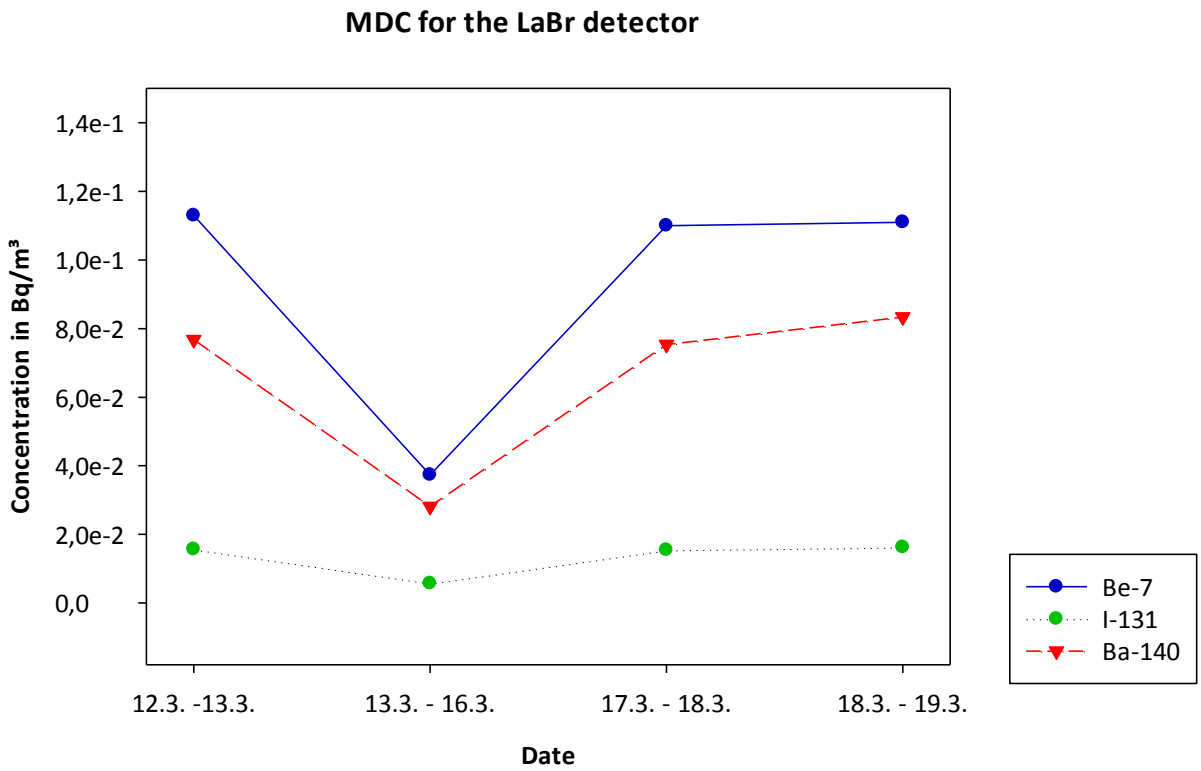

Figure 19 Variation of the MDC values during the March measurement. The tip in MDC values in the 2 measurement points (13.3. – 16.3.) derives from the longer collection time (see collection time Table 8).

7.2.2 Lead 214 results

The recorded activity variation of Pb-214 follows the expected variations very closely, which is described in chapter 4.1.2. The values of maximal measured activity in the air coincide with the time of sunrise. For the days between the 26th of June and the 4th of July 2015 this was between 4:55 and 5:00 o'clock (ZAMG, Auf- und Untergangszeiten von Sonne und Mond, 2015). The activity maxima that where recorded in the spectra during this time lay between 4 and 6 o'clock in the morning. Figure 20 shows the recorded diurnal variation, the average error of the activity is 4%. The error bars for the individual filters are shown in the more detailed curves shown in Appendix D. The increase from the daily minimum to the maximum was on average a fivefold.

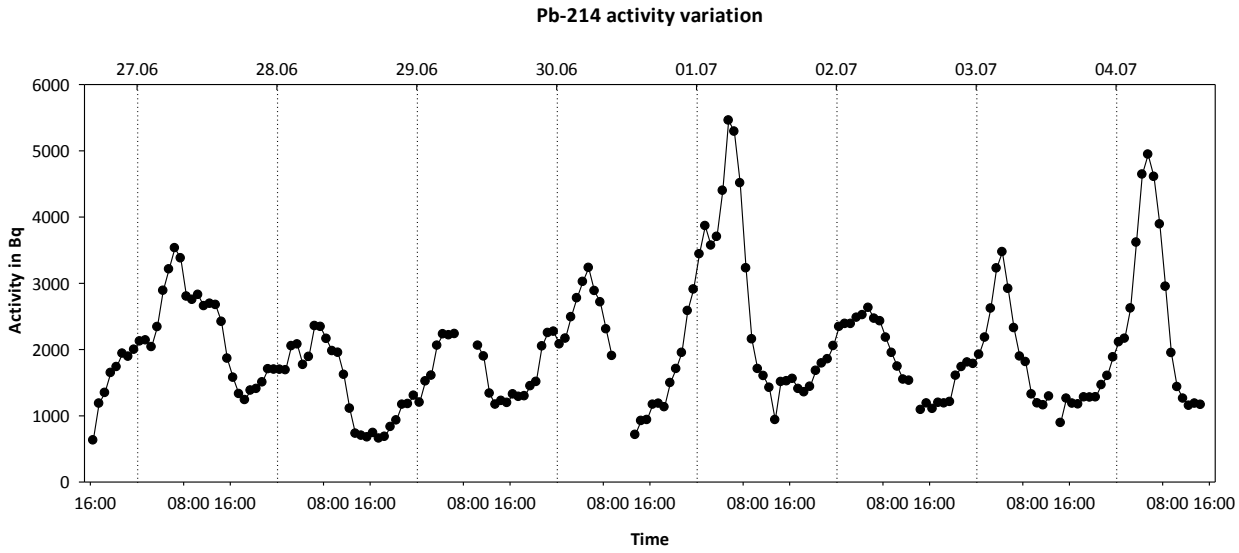

Figure 20 Pb-214 activity variation during the observed time period. The gaps in the graph are the times when no filter was in the station because of the filter changes. The expected diurinal variaton in the activity for Rn-222 daughters is clearly visible.

An interesting point is that, although the measurement was taken at a height of 118 m at the top of the VIC, the diurnal variation of the Radon daughter Pb-214 still distinctly follows the behaviour found by studies done near the ground (1-2 meters above ground).

A further distinct feature in Figure 20 is the unexpected slightly lower activity in the first spectra that where recorded after the filter was changed. The filter changes which were accompanied by a short measurement break are clearly visible because of the gaps in Figure 20. The fast filter change on the 1st of July at 13:30 which lead to a continuous measurement can be seen by the activity tip. The recorded precipitation on the 27th of June did not lead to a distinct reduction in the activity, although the first peak is not as well shaped as the later peaks.

The observed variation and the values of the peak centre and FWHM are shown in Table 9. One can see that the observed peak maximum is shifted slightly to a higher energy of 352.34 keV instead of 351.9 keV and that there are no diurnal variations that would be related to the environmental temperature. This is an indicator for the effectiveness of the automatic spectrum stabilisation of the system. See Figure 21.

Pb-214	Activity in Bq	Peak Centre in keV	FWHM in keV
Min	6.29E+02	351.15	12.20
Max	5.46E+03	353.14	15.71
Med	1.98E+03	352.34	13.48
Av	1.80E+03	352.34	13.52

Table 9 Variation of the activity, the peak center and FWHM of the Pb-214 peak recorded by the LaBr detector.

–

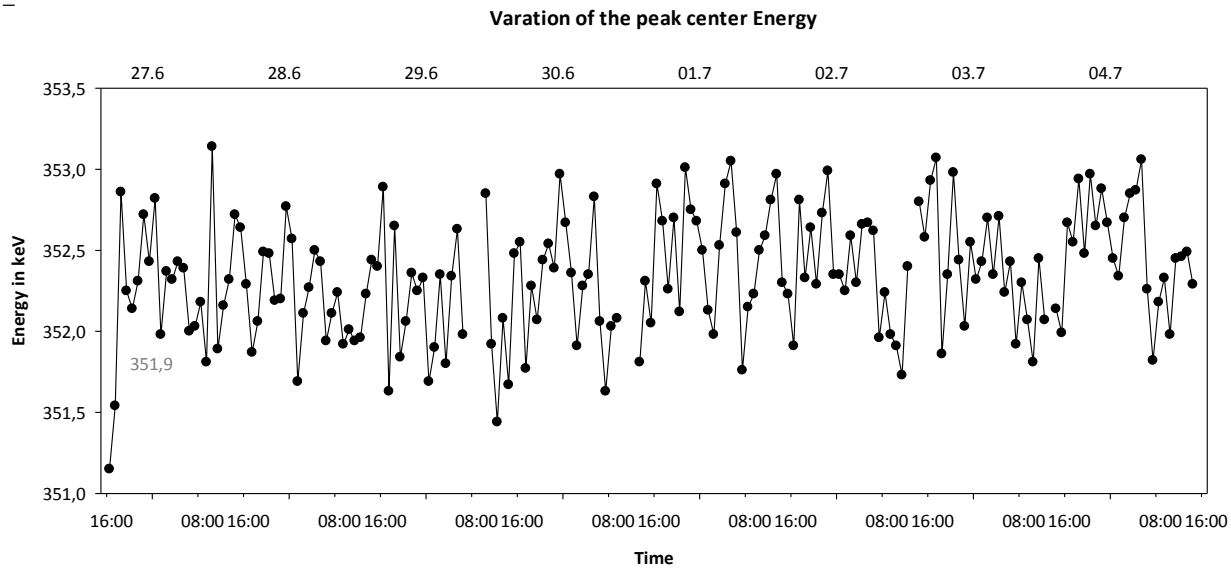

Figure 21 Variation of the peak energy of 351.9 keV peak of Pb-214 over time. The correct value of 351.9 is displayed as a dashed gray reference line.

The average FWHM value of 13.52 is only barely enough to enable a separation from the I-131 peak at 364.4 keV. Ideally the FWHM should be lower than 12.6 keV, as peaks are sufficiently resolved if they are at least one FWHM apart. This is achieved for some spectra, with an overall minimum FWHM at 12.2 keV. Nevertheless in the majority of the spectra the measured FWHM is below the value calculated from the energy calibration of 15.17 keV. The variation over time can be seen in Figure 22. There is a tendency for higher FWHM values in late afternoon hours around 8 pm. This is illustrated by the solid blue line, which represents the smoothed FWHM variation. This would also affect the variation of the peak centre energy if no correction by an automatic spectrum stabilisation was done.

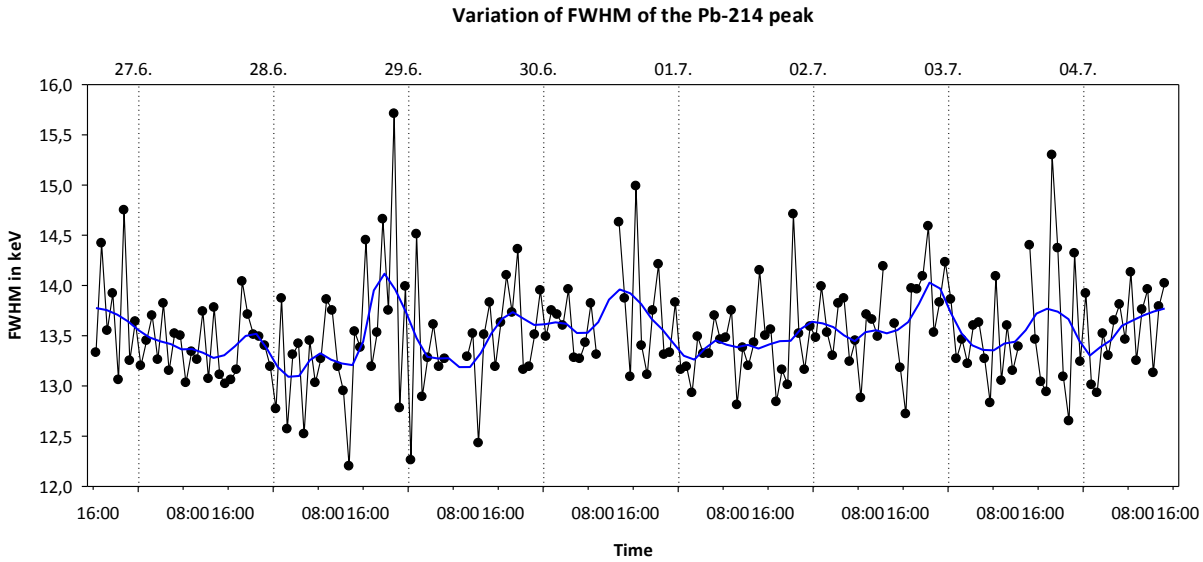

Figure 22 Variation of the FWHM of the 351.9 keV peak of Pb-214 over time. The smoothened curve is represented by the blue line. Clearly visible are the periodic peaks in the late afternoon before sunset.

The correlation between the detector temperature and the FWHM of the Pb-214 peak can be seen in Figure 23. It is visible that the high FWHM values correlate with the LaBr detector temperature, although the temperature of the detector peaks before the FWHM. The reason for the delayed FWHM maxima is not clear. Otherwise this behaviour follows the theoretical basis, as a higher detector temperature increases the uncertainties created by the detector and the electronics which are the reason for the peak width.

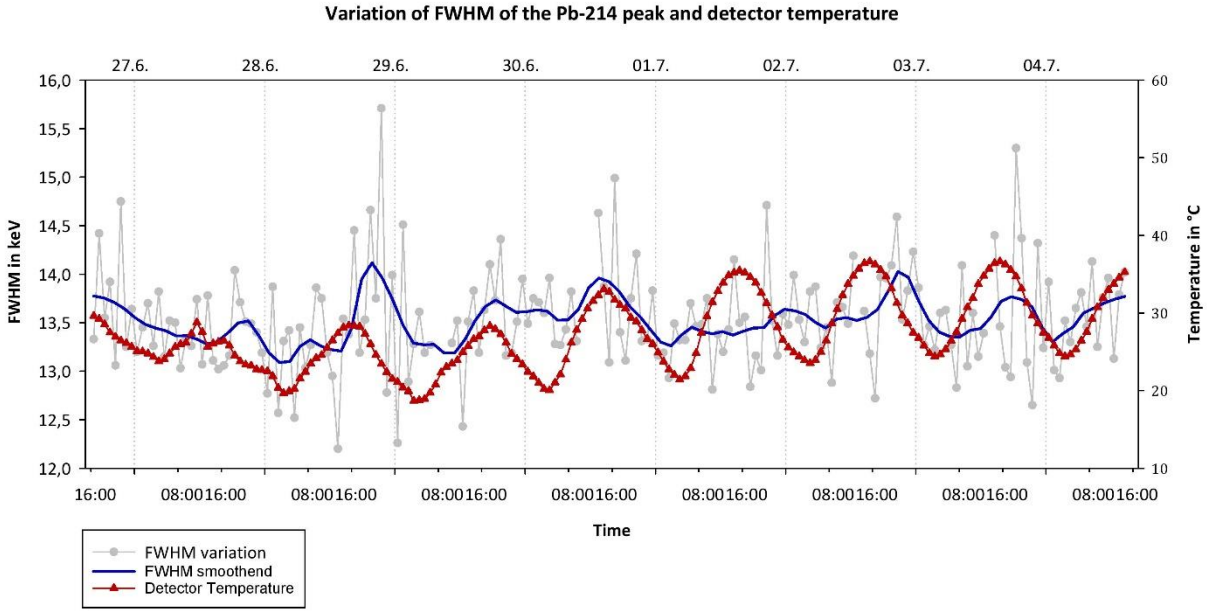

Figure 23 The blue line shows the smoothened variation of the FWHM. The red line shows the variation of the LaBr detector temperature. The sometimes delayed FWHM maximum compared the detector temperature is unexpected.

The diurnal variation of the Radon daughters also has an impact on the hourly MDC values. Since the further decay after Pb-214 to Pb-210, which has a half-life of 22.23 years, is rather quick (Bi-214 19.8 min, Po-214 162 µs) the spectrum background for the other nuclides of interest shows a variation over time that is related to the variation of Pb-214. For this MDC values are calculated with the hourly air flow of 800 m³ and not the total accumulated air flow of the filter. A detailed depiction for each nuclide over the observation time is shown in Appendix D.

7.3 Comparison of the LaBr results to the HPGe results

To compare the results of the two detectors regarding their MDC levels the values from the last spectra recorded by LaBr detector for each filter were taken. The comparison shows that the HPGe detector is overall more sensitive by an order of three. The direct comparison can be seen in Table 10.

Date	MDC in Bq/m³					
	Be-7		I-131		Ba-140	
	HPGe	LaBr	HPGe	LaBr	HPGe	LaBr
26.6. - 29.6.	6.81E-06	1.68E-02	1.55E-06	2.51E-03	4.92E-06	1.18E-02
29.6. - 30.6.	1.95E-05	4.14E-02	4.02E-06	6.09E-03	1.41E-05	3.06E-02
30.6. - 1.7.	2.18E-05	4.47E-02	4.49E-06	6.52E-03	1.57E-05	3.02E-02
1.7. - 2.7.	2.13E-05	4.30E-02	4.35E-06	6.44E-03	1.52E-05	3.07E-02
2.7. - 3.7.	2.17E-05	4.39E-02	4.53E-06	6.57E-03	1.61E-05	3.18E-02
3.7. - 4.7.	1.33E-05	3.81E-02	2.98E-06	6.05E-03	9.75E-06	2.91E-02

Table 10 Comparison of the MDV values from the HGPe and the LaBr detector.

In Figure 24 it can be seen that the concentration of Be-7, recorded with HPGe, is always below the calculated MDC level of the LaBr detector. Even for the first measurement filter on which the last measured spectra had a filter deposition time of around 60 hours, the measured concentration did not surpass the calculated MDC level of the LaBr detector. This leads to the conclusion that the natural concentration of Be-7 in the air, produced by cosmic radiation, cannot be detected with the LaBr detector.

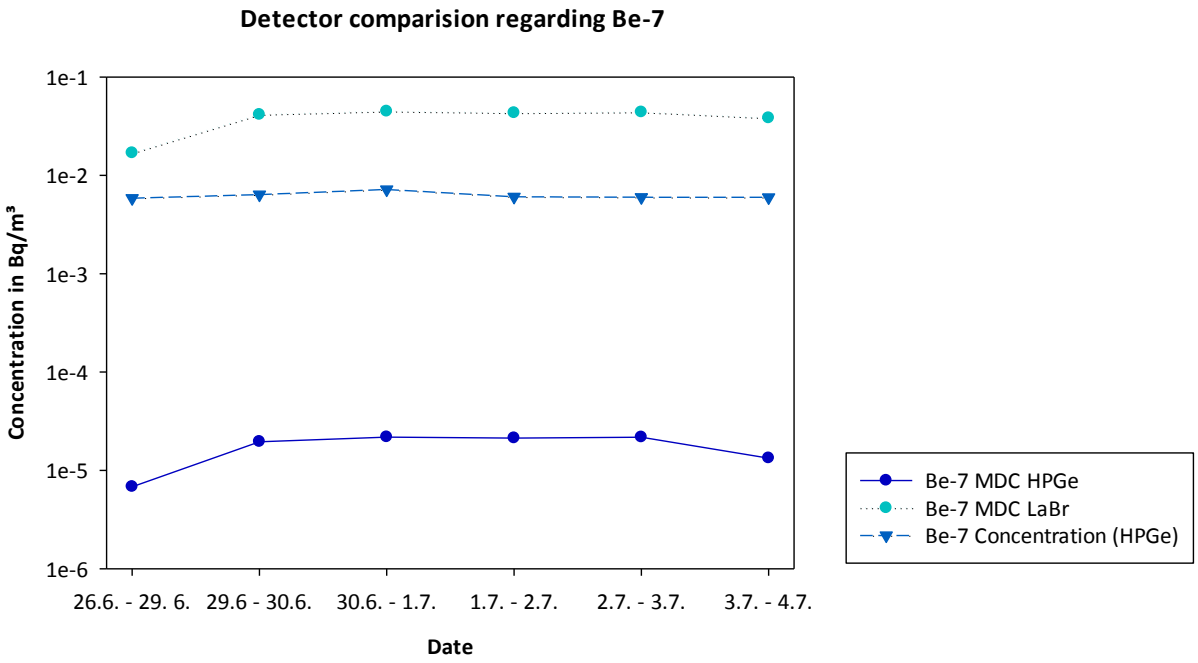

Figure 24 The Be-7 concentration recorded by the HPGe detector is significantly higher than its calculated MDC. However the MDC level calculated for the LaBr detector is always higher than the recorded Be-7 concentration.

However the diurnal variation of the short lived radioisotope Pb-214 can be observed very accurately with the LaBr detector. Whereas the HPGe detector can hardly detect this peak because it decays before the start of the acquisition time, to a level just above the MDC. Regarding the resolution of the Pb-214 peak to enable a satisfying distinction to I-131, the high base resolution of the HPGe detector can achieve this without having to rely on the strong decay of the Pb-214 peak. The LaBr detector fulfils the demand barely, as the FWHM of the Pb-214 peak reaches values of up to 15.7 keV. But the lowest measured FWHM of 12.2 keV is below the desired level of 12.6 keV.

8 Conclusions

8.1 Summary of the results and conclusions

The LaBr detector is not sensitive enough to measure the natural concentration of Be-7 (477.8 keV peak), neither for an acquisition time of 10 minutes nor for an acquisition time of one hour. However the diurnal variation of Pb-214 (351.9 keV peak) can be observed very well. Based on the position of the peak centroid and in combination with the according FWHM values it can be seen that the peak stabilisation, with the intrinsic La-138 peak, limits the effects temperature changes have on the detector. The peak centroid varies only about ±1 keV and the variations show no dependence on the environmental temperature. Whereas the FWHM values, which are as well temperature dependent, vary by more than 4 keV and show a distinct maximum in the late afternoon. The average resolution of 13.52 keV FWHM is barely enough to separate the Pb-214 351.9 keV peak from the I-131 364.5 keV peak. Because of the long timeframe between the collection and the start of the acquisition by the HPGe most of the Pb-214 is already decayed (half-life time of 26.9 min) and measured values are only slightly above the MDC level. The separation between the Pb-214 and the I-131 in HPGe detector spectra is no problem because of the much higher resolution of the HPGe detector compared to the LaBr detector.

The MDC levels of the one hour spectra from the LaBr detector are overall by three magnitudes higher than for the HPGe detector. The MDC level for the HPGe detector are between 10^{-6} Bq/m³ and 10^{-5} Bq/m³ whereas for the LaBr detector they are only 10^{-3} Bq/m³ to 10^{-2} Bq/m³ depending on the individual collection and decay times of the filters. This means that MDC for Ba-140 does not meet the demanded base line sensitivity of 10 to 30 µBq/m³ for the certification of an IMS particulate radionuclide stations. Also the I-131 values that where recorded after the Fukushima accident over Europe (1 - 6 mBq/m³) would be close to or slightly under the MDC level of the LaBr detector even after the full collection time of 24 hours. However high concentrations of 10 Bq/m³ which prevailed at measurement stations closer to an accident, such as in the assumed scenario in the motivation for the detector system, will be detected immediately, even in a 10 minute measurement. This enables the operator to handle such a filter with extra precautions to avoid radiologically hazardous situations for his/her health and adjust the station operation if necessary. The system can also provide the CTBTO with an early warning of unusually high

isotope activity concentrations in the air before the first preliminary spectra of the HPGe detectors are accessible (52 hours after the collection started).

8.2 Further steps

In further measurements with the LaBr system the efficiency calibration should take place after the spectra are converted into CNF files with the RMS Data Viewer to ensure their accuracy. Or the rounding problem has to be corrected within the RMS Data Viewer itself. This issue extends to all spectra that receive calibrations before they are converted by the RMS Data Viewer, not only the spectra from the LaBr detector.

An increase of the measurement time of the LaBr detector beyond one hour is only of limited benefit. The concentration variation of Pb-214 would no longer be recordable in precision. The possible increase in isotope concentration to reach values above the MDC limit and enable the measurement of the natural Be-7 concentration in the air is unlikely. This could easily by verified by doing a set of longer measurements that decline in time if the previous one should actually reach a low enough MDC level for Be-7. But a permanent increase in measurement time would deny the quick feedback for high activity concentrations on the filter from dangerous events with high radionuclide releases.

To gain definitive results whether the LaBr detector can resolve and correctly detect Ba-140 and I-131 in concentrations that impose a danger to the station operator or even match expected values for nuclear accidents or nuclear weapon tests, a test measurement with consecutive one hour measurements of a primed filter could be done.

To enhance the assessment of the gained activity concentration and activity variations from the recorded nuclides the weather station that is mounted on the Snow Whit air sampler can be used. This data can be tied into other weather data from the region of Vienna to get a more complete picture. This is of interest for every isotope that is cleared from the air by wet deposition, including Pb-214 and Be-7.

To gain a more complete relation between the measured peak centroid and FWHM variation with the LaBr detector temperature, especially for the 351.9 keV Pb-214 peak, it would be of interest to gather data for a longer period of time (e. g. several weeks).

Since the LaBr detector system is currently not operational and an upgrade for the operating software is anticipated these steps are put on hold for the time being.

9 References

Atomicarchive.com, Radioactive Fallout.

http://www.atomicarchive.com/Effects/effects17.shtml [1.12.2015]

Canberra Industries, Inc. (2013). Broad Energy Germanium Detectors (BEGe). Available from:

http://www.canberra.com/products/detectors/pdf/BEGe-SS-C40426.pdf

[30.11.2015]

Canberra Industries, Inc. (2014). Germanium Detectors.
http://www.canberra.com/products/detectors/pdf/Germanium-Det-SS-C39606.pdf.
[30.11.2015]

Canberra Industries, Inc. (2011). Detector Specification and Performance Data

Canberra Industries, Inc. (2014). Detector Specification and Performance Data After Repair

Cannizzaro, F., Greco, G., Raneli, M., Spitale, M.C., Tomarchio, E. (2004). Concentration measurements of ^{7}Be at ground level air at Palermo, Italy - comparison with solar activity over a period of 21 years. Journal of Environmental Radioactivity 72, 259-271

CTBTO, Introduction to Radionuclide Monitoring Technology. Available from:

http://foresight.ctbto.org/download/attachments/9207840/03D+Introduction+to+Radionuclide+Monitoring+Technology.pdf [1.12.2015]

Faber, M., Leeb, H. (2011). Atom-, Kern-, und Teilchenphysik I. 142.086 Atom-, Kern- und Teilchenphysik I, 2012, Technische Universität Wien

French, N. R. (1963). Review and discussion of barium. In: Schultz, V., Klement, A. W. Jr. (Eds.) Radioecology, Proceedings of the First National Symposium on Radioecology held at Colorado State University, Fort Collins, Colorado, September 10-15, 1961. 557-560

Gilmore, R. G. (2008). Practical Gamma-ray Spectrometry (2nd Edition.). Chichester: Wiley & Sons

IAEA, C-3 Cumulative Fission Yields. https://www-nds.iaea.org/sgnucdat/c3.htm
[30.11.2015]

Khrustalev, K., Radulescu, I., Gelashvili, V., Strobl, F.-S. (2015). LaBr Online Filter Monitoring System: testing results and future project. Science and Technology 2015, Vienna, Austria, 22. – 26.6.2015

Klement, A. W. Jr. (1959). A review of potential radionuclides produced in weapons detonations. Washington, D. C.: U. S. Atomic Energy Commission

Kulan, A., Aldahan, A., Possnert, G., Vintersved, I. (2006). Distribution of ^{7}Be in surface of Europe. Atmospheric Environment 40, 3855-3868

Laboratoire National Henri Bequerel,Recommended data (by Z). http://www.nucleide.org/DDEP_WG/DDEPdata_by_Z.htm [1.12.2015]

Laboratoire National Henri Bequerel, by Helmer, R. G., Schönfeld, E. (2004). ^{7}Be. Available from: http://www.nucleide.org/DDEP_WG/DDEPdata_by_Z.htm [1.12.2015]

Laboratoire National Henri Bequerel. by Chisté, V., Bé, M.-M. (2014). ^{131}I. Available from: http://www.nucleide.org/DDEP_WG/DDEPdata_by_Z.htm [1.12.2015]

Laboratoire National Henri Bequerel. Bé, M.-M. (2014). ^{138}La. Available from: http://www.nucleide.org/DDEP_WG/DDEPdata_by_Z.htm [1.12.2015]

Laboratoire National Henri Bequerel. By Helmer, R.G. (2008). ^{140}Ba. Available from: http://www.nucleide.org/DDEP_WG/DDEPdata_by_Z.htm [1.12.2015]

Laboratoire National Henri Bequerel. by Chisté, V., Bé, M.-M. (2010). ^{214}Pb. Available from: http://www.nucleide.org/DDEP_WG/DDEPdata_by_Z.htm [1.12.2015]

Lal, D., Peters, B. (1969). Cosmic ray produced radioactivity on the Earth. In: Sittle, K. (Ed.). Handbuch der Physik. Vol. 46. Berlin, Springer, 551-612

Martin, J. E. (2006). Physics for radiation protection: a handbook. Wiley-VCH

Masarik, J., Beer, J. (1999). Simulation of particle fluxes and cosmogenic nuclides production in earth's atmosphere. Journal of Geophysical Research 104, 12099-12112

O. Masson, Baeza, A., Bieringer, J., Brudecki, K., Bucci, S., Cappai, M., Carvalho, F.P., Connan, O., Cosma, C., Dalheimer, A., Didier, D., Depuydt, G., De Geer, L.E., De Vismes, A., Gini, L., Groppi, F., Gudnason, K., Gurriaran, R., Hainz, D., Halldórsson, Ó., Hammond, D. Hanley, O., Holeý, K., Homoki, Zs., Ioannidou, A., Isajenko, K., Jankovic, M., Katzlberger, C., Kettunen, M., Kierepko, R., Kontro, R., Kwakman, P.J.M., Lecomte, M., Leon Vintro, L., Leppänen, A.-P., Lind, B., Lujaniene, G., Mc Ginnity, P., Mc Mahon, C., Malá, H., Manenti, S., Manolopoulou, M., Mattila, A., Mauring, A., Mietelski, J.W.,

Møller, B., Nielsen, S.P. Nikolic, J., Overwater, R.M.W. Pálsson, S. E., Papastefanou, C., Penev, I., Pham, M.K., Povinec, P.P., Ramebäck, H., Reis, M.C., Ringer, W., Rodriguez, A., Rulík, P., Saey, P.R.J., Samsonov, V., Schlosser, C., Sgorbati, G., Silobritiene, B. V., Söderström, C., Sogni, R., Solier, L., Sonck, M., Steinhauser, G., Steinkopff, T., Steinmann, P., Stoulos, S., Sýkora, I., Todorovic, D., Tooloutalaie, N., Tositti, L., Tschiersch, J., Ugron, A., Vagena, E., Vargas, A., Wershofen, H., Zhukova, O. (2011). Tracking of Airborne Radionuclides from the Damaged Fukushima Dai-Ichi Nuclear Reactors by European Networks. Environmental Science and Technology 45, 7670–7677

Nagaraja, K., Prasad, B.S.N., Madhava, M.S., Chandrashekara, M.S. Paramesh, L., Sannappa, J. Pawar, S.D., Murugavel, P. Kamra, A.K. (2003). Radon and its short-lived progeny: variations near the ground. Radiation Measurements 36, 413 - 417

NASA, Solar Cycle Prediction. available at: http://solarscience.msfc.nasa.gov/predict.shtml [1.12.2015]

Papastefanou, C. (2009). Radon Decay Product Aerosols in Ambient Air Aerosol and Air Quality Research 9, 385-393

Pruthvi Rani, K.S., Paramesh, L., Chandrashekara M.S. (2014). Diurnal variations of ^{218}Po, ^{214}Pb, and ^{214}Po and their effect on atmospheric electrical conductivity in the lower atmosphere at Mysore city, Karnataka State, India. Journal of Environmental Radioactivity 138, 438-443

Radulescu, I. (2015). Private correspondence 25.9.2015

Rulík, P., Malátová, I., Drábová, D., Tomášek, M. (2005). Long Term Observation of ^{137}Cs, ^{7}Be, ^{210}Pb and ^{40}K in the Air Aerosol and ^{85}Kr in the Air in Prague, Czech Republic. Available from: http://www.irpa.net/irpa10/cdrom/00528.pdf [1.12.2015]

Saint-Gobain Ceramics & Plastics, Inc. (2014). BrilLanCe 380 Data Sheet, available from: http://www.crystals.saint-gobain.com/uploadedFiles/SG-Crystals/Documents/BrilLanCe%20380%20Data%20Sheet.pdf [1.12.2015]

Saint-Gobain Ceramics & Plastics, Inc. (2009). SGC BrilLanCe Scintillators Performance Summary. available from: http://www.crystals.saint-gobain.com/uploadedFiles/SG-

Crystals/Documents/Technical/SGC%20BrilLanCe%20Scintillators%20Performance%20Summary.pdf [1.12.2015]

Saint-Gobain Ceramics & Plastics, Inc. (2014). Efficiency Calculations for Selected Scintillators. Available from: http://www.crystals.saint-gobain.com/uploadedFiles/SG-Crystals/Documents/Technical/SGC%20Efficiency%20Calculations%20Brochure.pdf

Senya. (2009). High Volume Air Sampler SNOW WHITE. Available from: http://www.senya.fi/manuals/docs/ManualMAWS.pdf?snow_pos=QML201%20%E2%89%A5%202009& [1.12.2015]

Spaceweatherlive. Sonnenzyklus Progression. http://www.spaceweatherlive.com/de/sonnenaktivitat/sonnenzyklus-progression. [30.11.2015]

Sesana, L., Caprioli, E. Marcazzan, G.M. (2003). Long period study of outdoor radon concentration in Milan and correlation between its temporal variations and dispersion properties of atmosphere. Journal of Environmental Radioactivity 65, 147–160

Steinmann, P., Zeller, M., Beuret, P.,Ferreri, G., Estier, S. (2013). Cosmogenic ^{7}Be and ^{22}Na in ground level air in Switzerland (1994-2011). Journal of Environmental Radioactivity 124, 68-73

Seftelis, I., Nicolaou, G., Trassanidis, S., Tsagas, F.N. (2007). Diurnal variation of radon progeny. Journal of Environmental Radioactivity 97, 116-123

Stohl, A., Bonasoni, P., Cristofanelli, P., Collins, W., Feichter, J., Frank, A., Forster, C., Gerasopoulos, E., Gäggeler, H., James, P., Kentarchos, T., Kromp-Kolb, H., Krüger, B., Land, C., Meloen, J., Papayannis, A., Priller, A., Seibert, P., Sprenger, M., Roelofs, G.J., Scheel, H.E., Schnabel, C., Siegmund, P., Tobler, L., Trickl, T., Wernli, H., Wirth, V., Zanis, P., Zerefos, C. (2003). Stratosphere-troposphere exchange: a review, and what we have learned from STACCATO. Journal of Geophysical Research 108 (D12), 8516

University of Natural Resources and Life Sciences, Vienna. Monatsübersicht Wetterstation BOKU-Met Juni 2015. https://meteo.boku.ac.at/wetter/mon-archiv/2015/201506/201506.html#img_ns. [30.11.2015]

U.S. Department of Health and Human Services / Agency for Toxic Substances and Disease Registry. (2007). Toxicological Profile for Barium and Barium Compounds.

U.S. Department of Health and Human Services / Agency for Toxic Substances and Disease Registry. (2004). Toxicological Profile for Iodine

Wilson, B.J. (1966). The Radiochemical Manual, 2nd Edition. Amersham: The Radiochemical Centre. Available from: https://archive.org/details/TheRadiochemicalManual [1.12.2015]

Zanis, P., Gerasopoulos, C., Priller, A., Schnabel, C., Zerefos, C., Gäggeler, H.W., Tobler, L., Kubik, P.W., Berger, M., Kanter, H.J., Scheel, H.E., Luterbach, J., Stohl, A. (2003). An estimate of the impact of stratosphere-to-troposphere transport (STT) on the lower free tropospheric ozone over the Alps using ^{10}Be and ^{7}Be measurements. Journal of Geophysical Research 108 (D12), 8520

ZAMG Zentralanstalt für Meteorologie und Geodynamik. Auf- und Untergangszeiten von Sonne und Mond. https://www.zamg.ac.at/cms/de/klima/klimauebersichten/ephemeriden [1.12.2015]

ZAMG Zentralanstalt für Meteorologie und Geodynamik. Monatsrückblick, Juni und Juli 2015. http://www.zamg.ac.at/cms/de/klima/klima-aktuell/monatsrueckblick/wetterrueckblick/?jahr=2015. [30.11.2015]

10 Appendix

A. Decay schemes

Pb-214

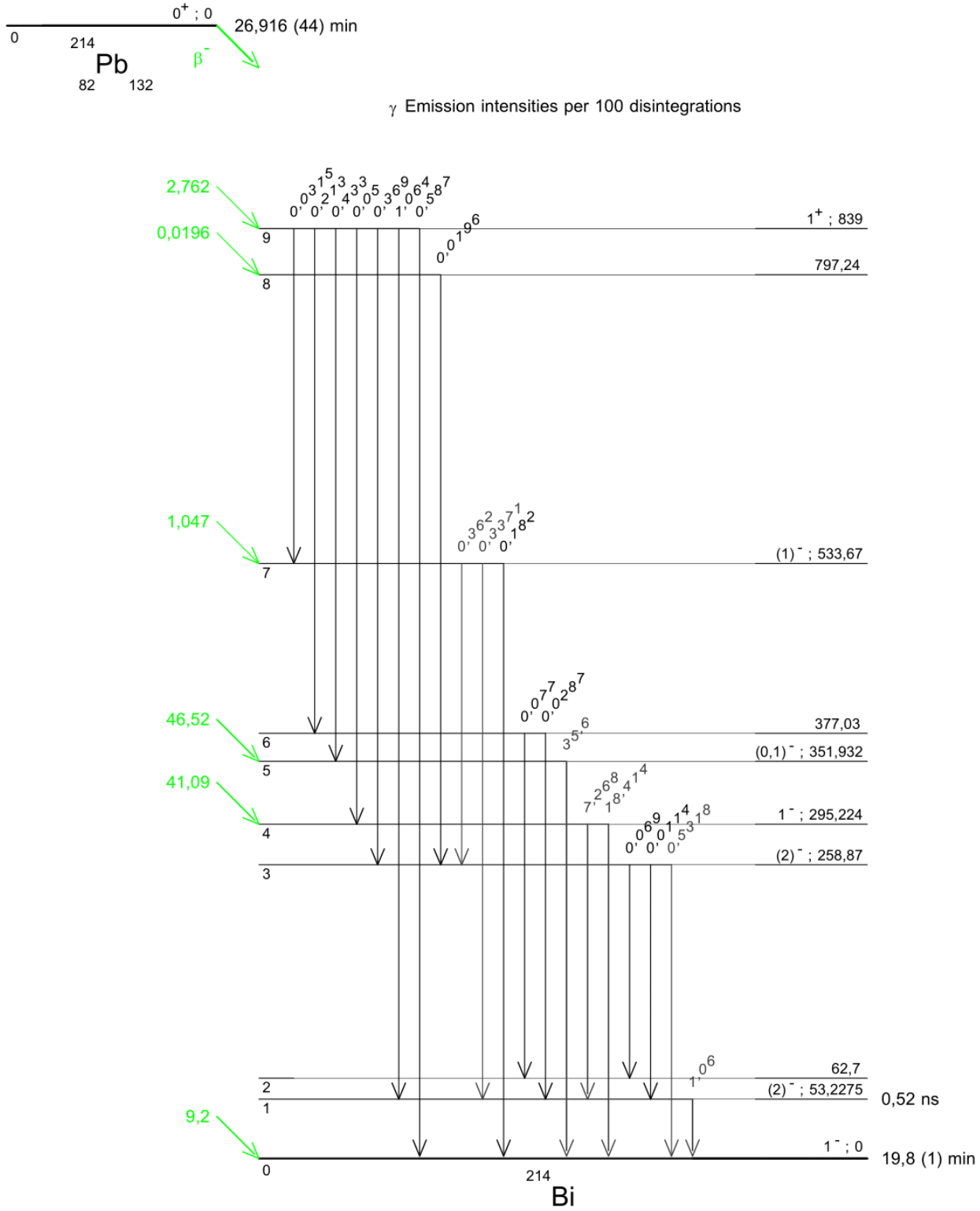

Figure 25 Decay scheme of Pb-214 with all possible decay paths and their probabilities. (Laboratoire National Henri Bequerel, ^{214}Pb, 2010)

Be-7

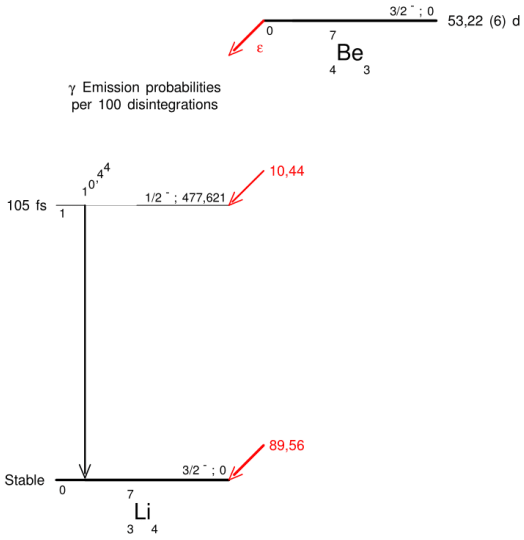

Figure 26 Schematic of the decay path of Be-7. (Laboratoire National Henri Bequerel, ^{7}Be, 2004)

Ba-140

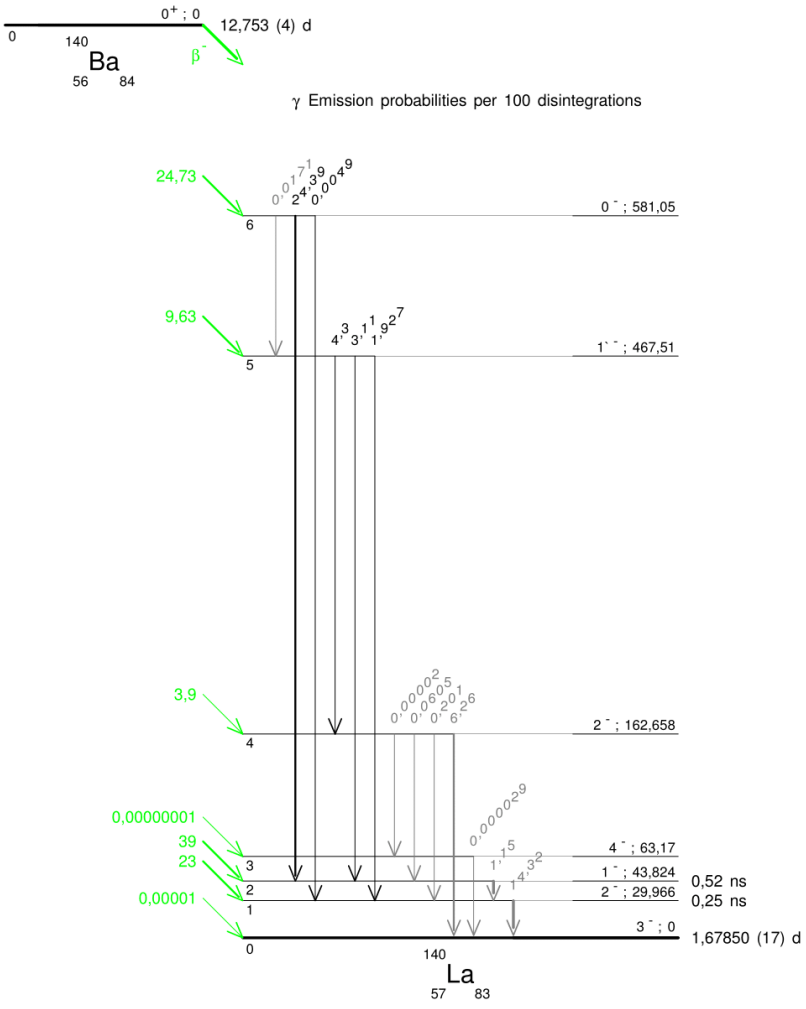

Figure 27 Schematic decay path of Ba-140. (Laboratoire National Henri Bequerel, ^{140}Ba, 2008)

I-131

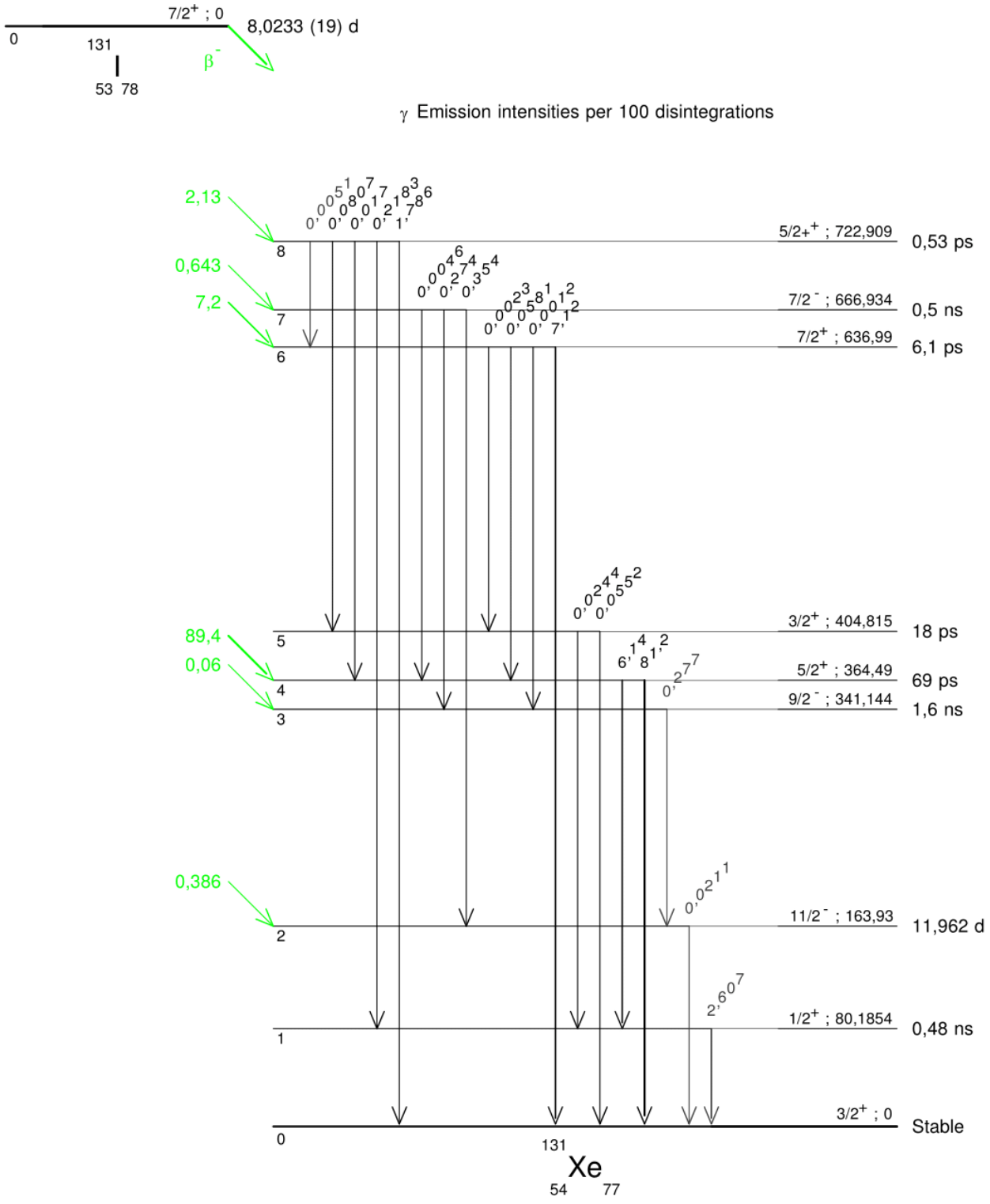

Figure 28 Schematic of the decay path of I-131. . (Laboratoire National Henri Bequerel, ^{131}I, 2014)

B. Certification data for the HPGe detector calibration

The entries in the calibration block stand for following physical values:

#Certificate

Total source activity (Bq) Assay date (yyyy/mm/dd) Assay time (hh:mm:ss) Nuclide name Half-life time Activity at time of assay Uncertainty (%) γ-Energy (keV) γ-Intensity (percent) Electron decay mode descriptor maximum β-particle energy or Ce energy (keV) Intensity of the β-particle (percent)

#Certificate

9218 2014/06/01 12:00:00.0

PB-210	22.3000 Y	1202.000	12.810	46.539	4.250	0 0 0
AM-241	432.2000 Y	295.300	4.601	59.541	35.900	0 0 0
CD-109	462.6000 D	1645.000	54.195	88.034	3.700	0 0 0
CO-57	271.7900 D	60.300	0.514	122.061	85.600	0 0 0
CO-57	271.7900 D	60.300	0.674	136.474	10.680	0 0 0
CE-139	137.6410 D	67.700	0.700	165.857	79.900	0 0 0
CR-51	27.7030 D	2935.000	29.093	320.083	9.870	0 0 0
SN-113	115.0900 D	273.200	2.697	391.698	64.970	0 0 0
SR-85	64.8400 D	217.900	2.000	514.007	95.712	0 0 0
CS-137	30.0400 Y	315.800	2.849	661.657	85.100	0 0 0
MN-54	312.3000 D	284.900	1.749	834.848	99.976	0 0 0
Y-88	106.6500 D	488.200	3.423	898.042	93.683	0 0 0
ZN-65	244.0600 D	611.000	5.660	1115.539	50.600	0 0 0
CO-60	5.2710 Y	333.900	1.853	1173.228	99.850	0 0 0
CO-60	5.2710 Y	333.900	1.850	1332.492	99.983	0 0 0
Y-88	106.6500 D	488.200	3.385	1836.063	99.240	0 0 0
CO-60	5.2710 Y	333.900	1.967	2505.692	0.000	0 0 0
Y-88	106.6500 D	488.200	3.051	2734.105	0.010	0 0 0

C. Efficiency calibration data of the LaBr detector

#g_Efficiency

keV	Calculated Efficiency	Measured Efficiency
59.5	0.00288	0.00014
122.1	0.00356	0.00018
165.9	0.00334	0.00017
320.1	0.00163	0.00007
391.7	0.00141	0.00007
514	0.00126	0.00009
661.6	0.00103	0.00005
834	0.00074	0.00004
898	0.00072	0.00004
1115.6	0.00057	0.00004
1173.2	0.00046	0.00003
1332.5	0.00035	0.00003
1836.1	0.00025	0.00002

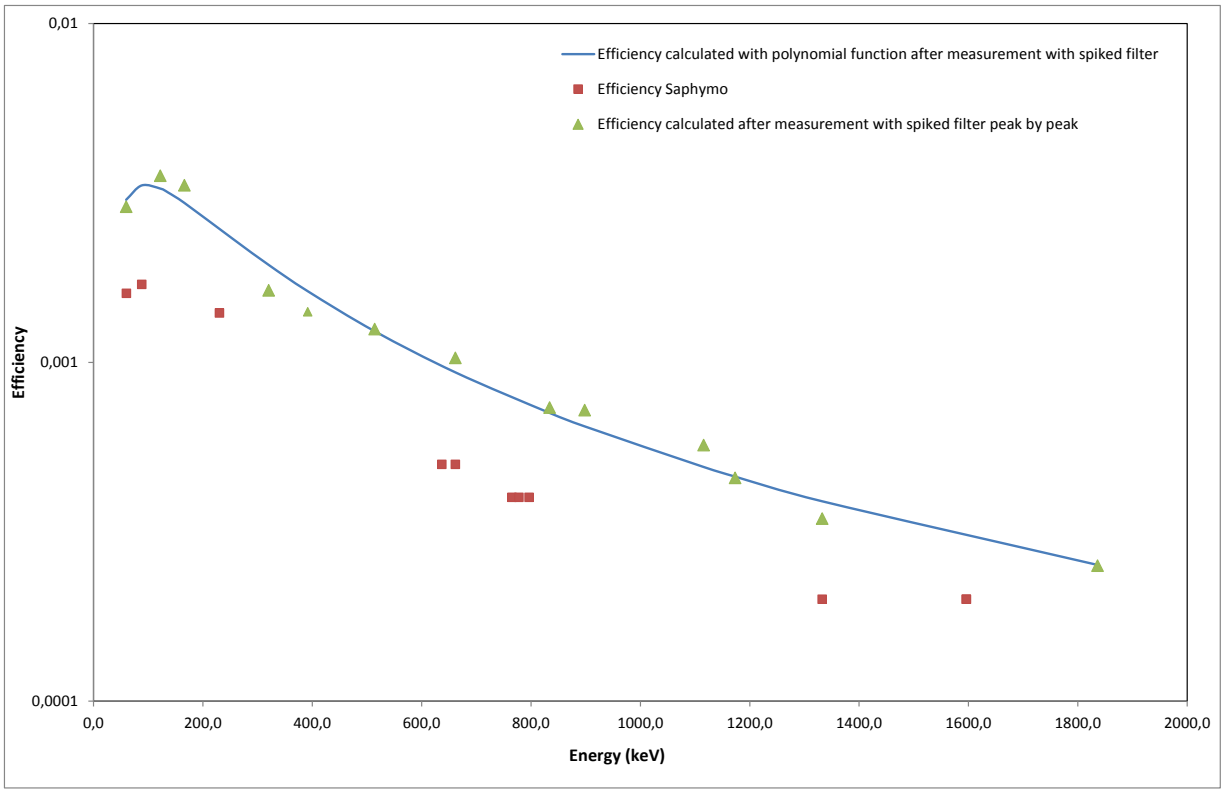

Figure 29 Efficiency calibration gained from a 7.5 hour long measurement with a calibration filter. Done and provided by Ileana Radulescu.(Radulescu, 2015)

D. Detailed results of for the individual days from the LaBr spectra

Minimal Detectable Concentration for the last 6 measurements

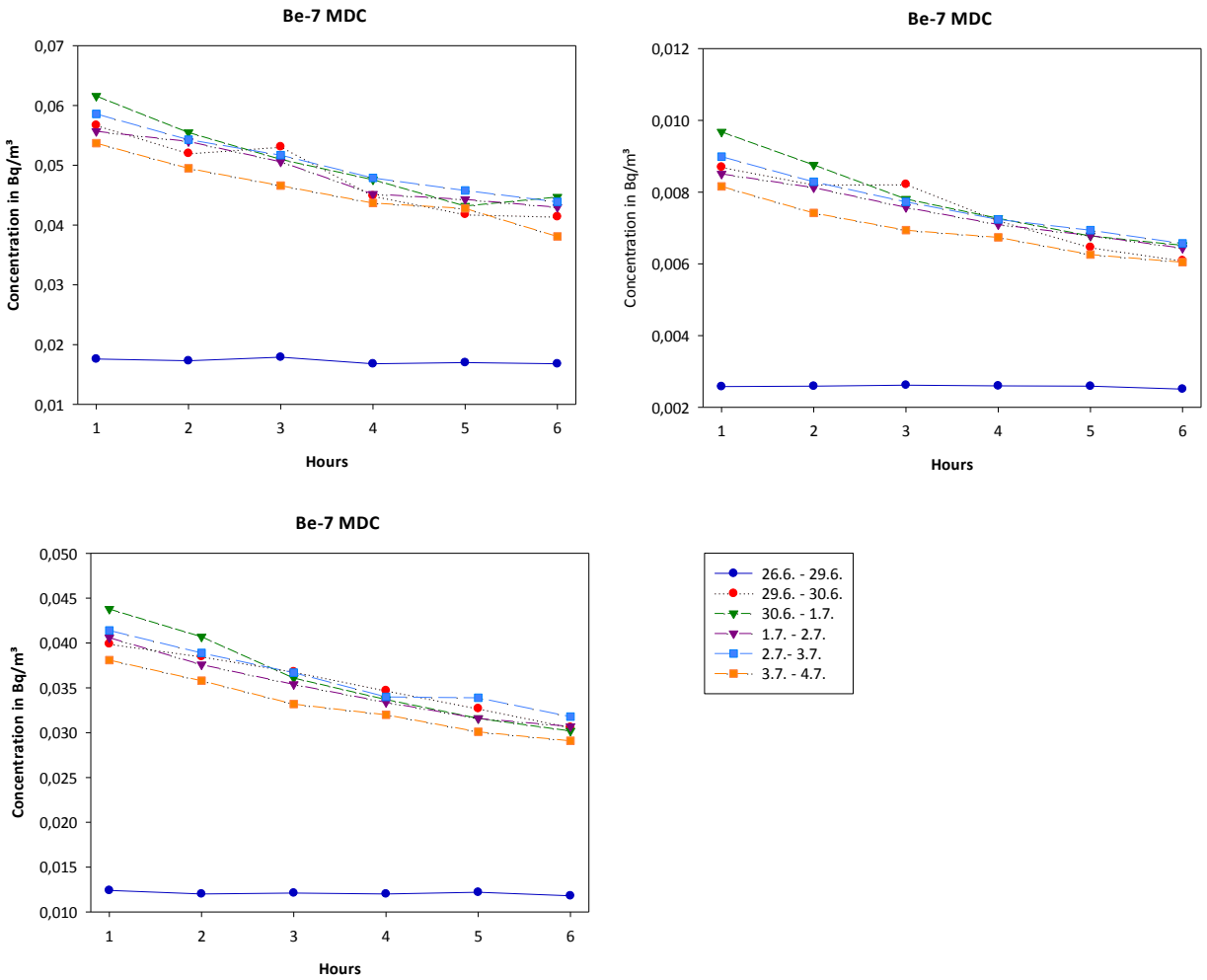

Figure 30 MDC values for the last 6 hours before a filter change.The significantly lower values for the results from the 26.6. - 29.6.2015 derive from the longer collection time (nearly 3 days).

Activity of Pb-214 on the specific days

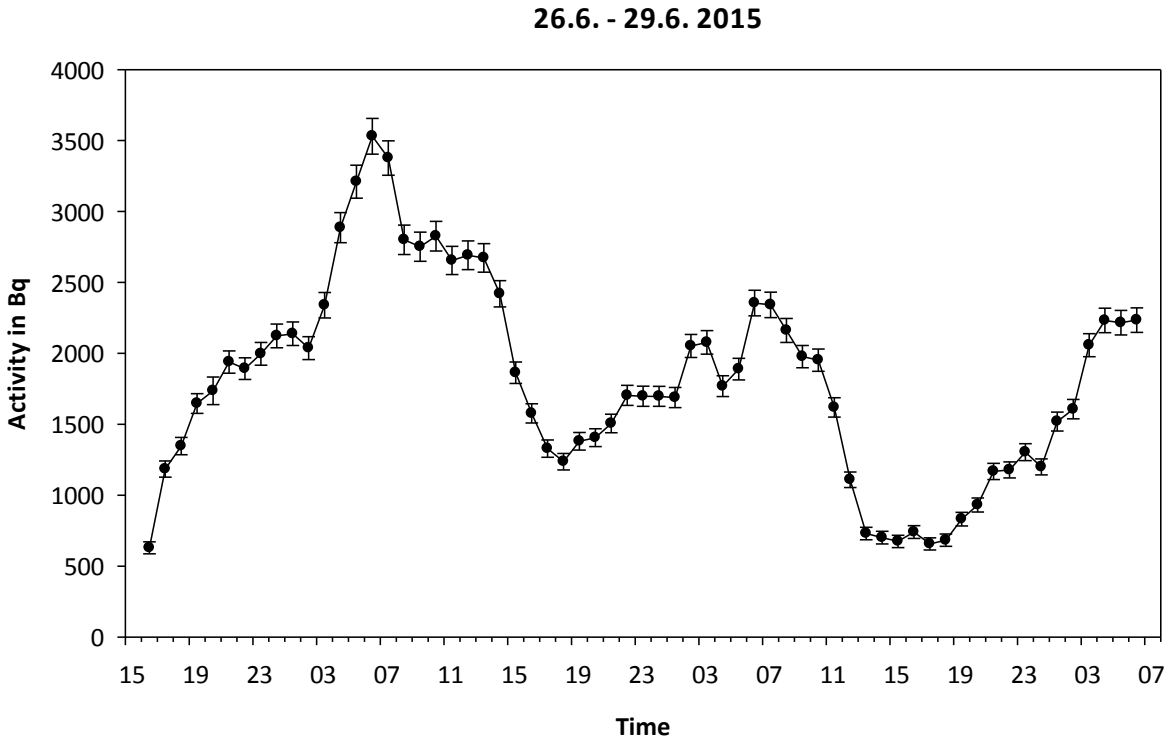

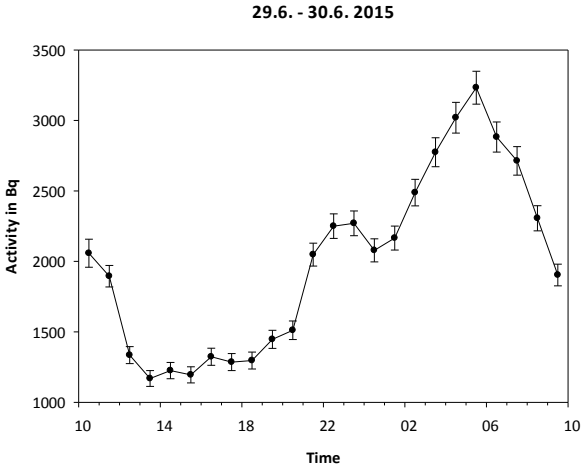

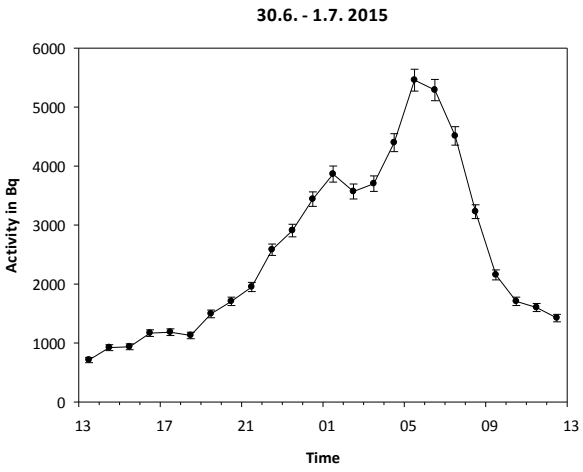

1.7. - 2.7. 2015

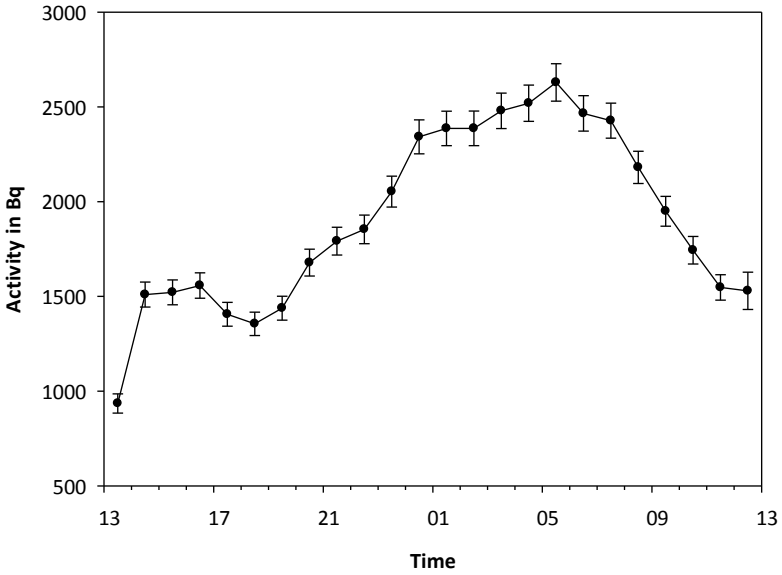

2.7. - 3.7. 2015

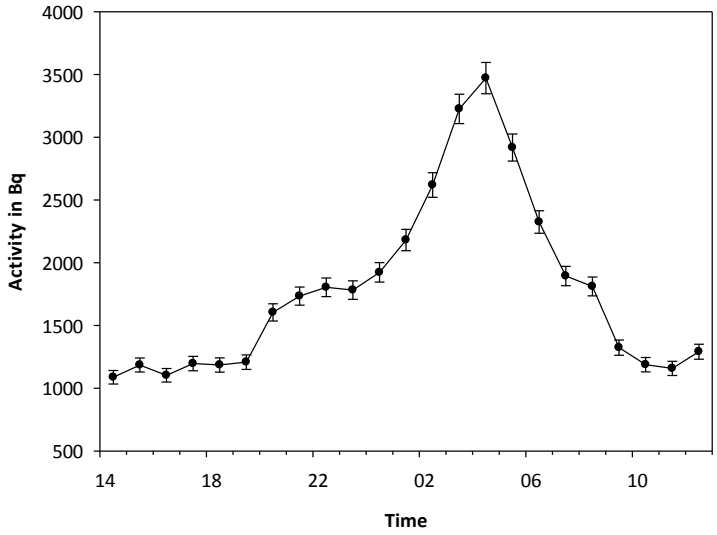

2.7. - 3.7. 2015

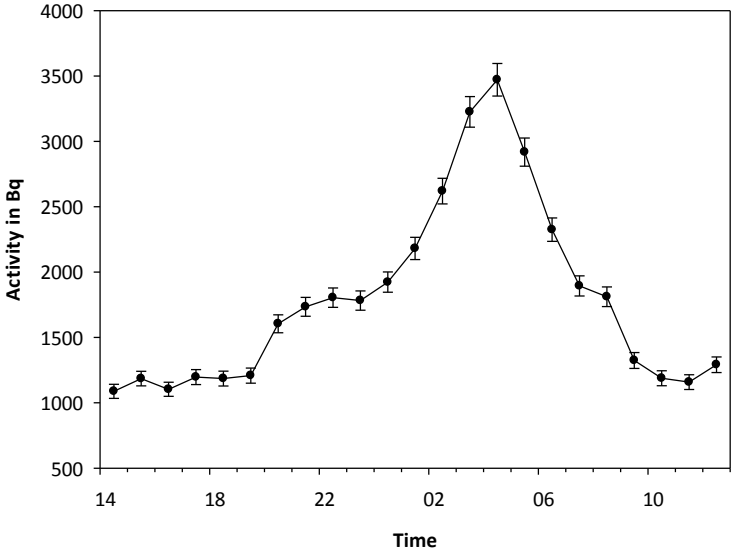

Variation of the hourly MDC value (air flow of 800 m³) with the activity variation of Pb-214

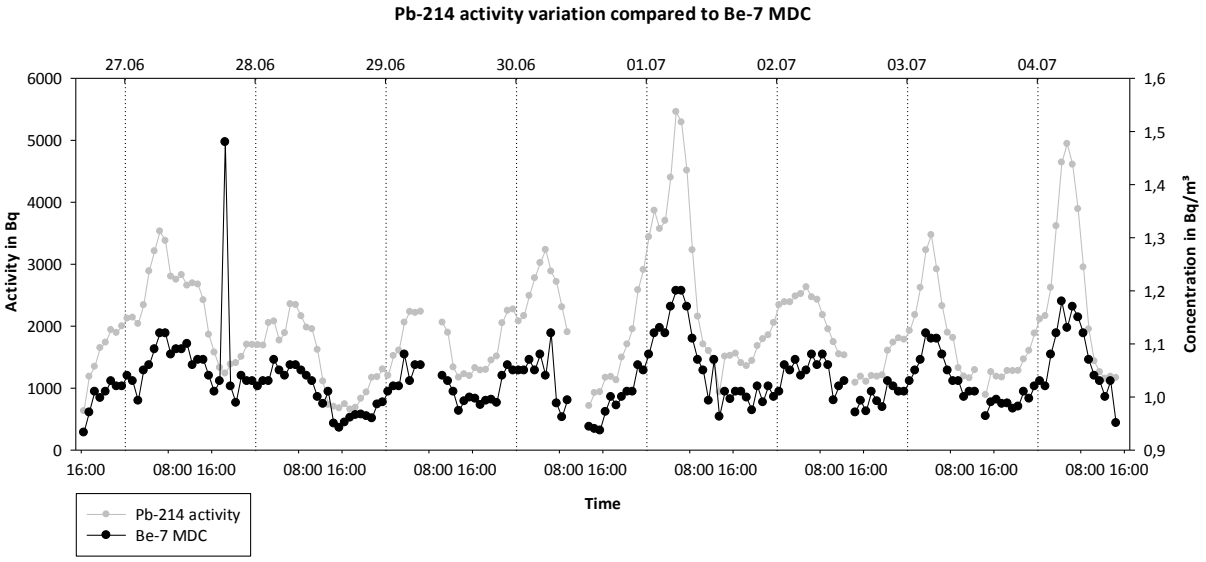

The very high MDC value for the 27th measurement point at 18:30 derives from a high count region in the area of 460 keV that spreads into the ROI of the Be-7 peak. This is the only time that such a property is observed and therefore it is regarded as a random artefact.

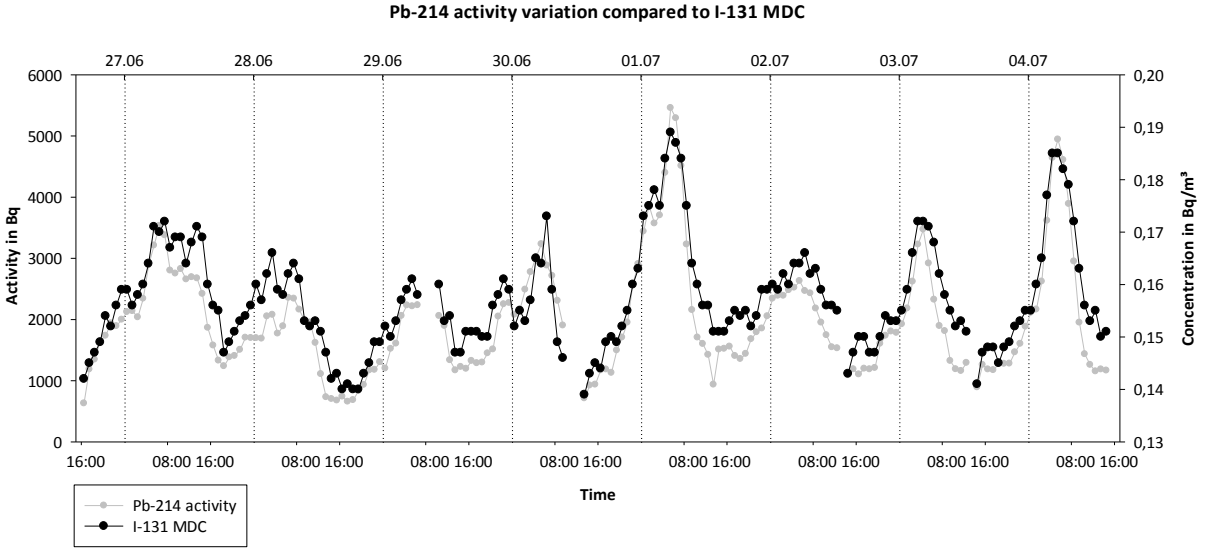

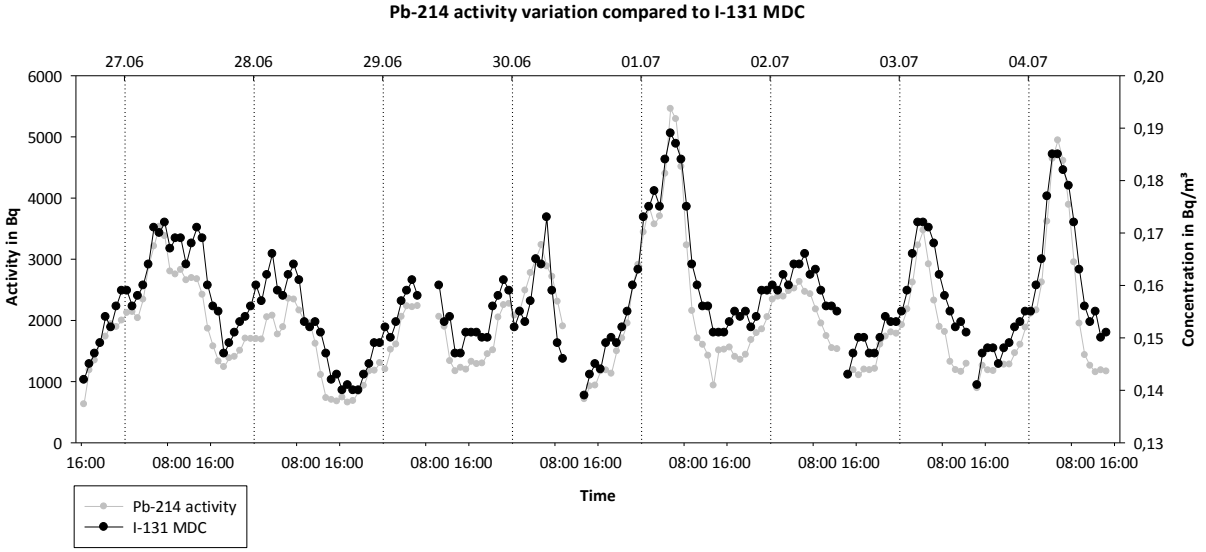

E. Exemplary peak plots for the HPGe detector

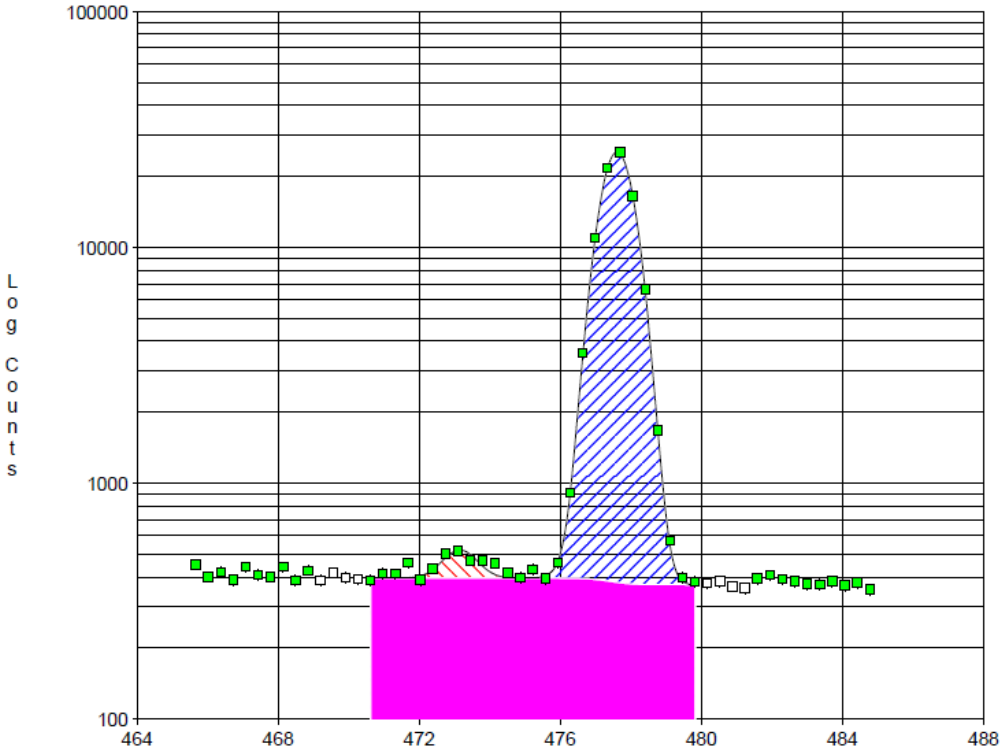

Figure 31 Be-7 477.8 keV peak in the HPGe spectrum taken from the filter 2.-3.7.2015. The peak is clearly visible and well-shaped.

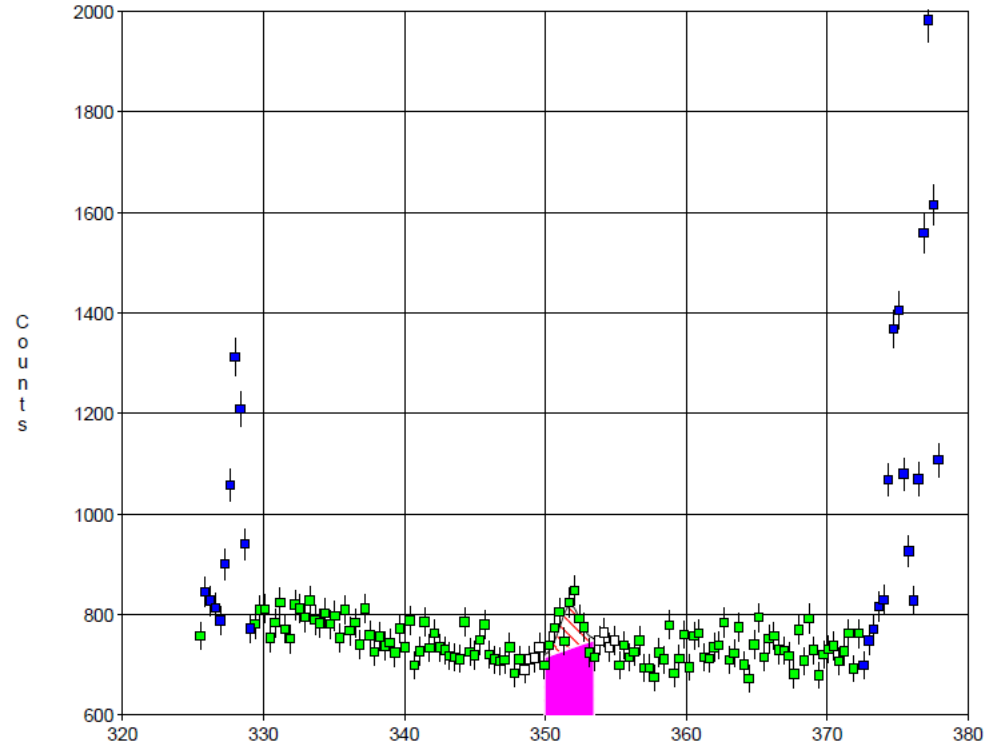

Figure 32 Pb-214 351.9 keV peak in the HPGe spectrum from the filter collected on 2.-3.7.2015. The peak is already strongly decayed and its remaining shape is not very pronound. The MDC limit was 1.1562E-05 Bq/m³ and the detected concentration was just above this limit with 1.4461E-05.